iScience

CellPress
OPEN ACCESS

Review

Junction and energy band on novel semiconductor-based fuel cells

Enyi Hu,[1] Zheng Jiang,[1] Liangdong Fan,[2,*] Manish Singh,[3] Faze Wang,[1] Rizwan Raza,[4,5,*] Muhammad Sajid,[4] Jun Wang,[1] Jung-Sik Kim,[6,*] and Bin Zhu[1,6,*]

SUMMARY

Fuel cells are highly efficient and green power sources. The typical membrane electrode assembly is necessary for common electrochemical devices. Recent research and development in solid oxide fuel cells have opened up many new opportunities based on the semiconductor or its heterostructure materials. Semiconductor-based fuel cells (SBFCs) realize the fuel cell functionality in a much more straightforward way. This work aims to discuss new strategies and scientific principles of SBFCs by reviewing various novel junction types/interfaces, i.e., bulk and planar p-n junction, Schottky junction, and n-i type interface contact. New designing methodologies of SBFCs from energy band/alignment and built-in electric field (BIEF), which block the internal electronic transport while assisting interfacial superionic transport and subsequently enhance device performance, are comprehensively reviewed. This work highlights the recent advances of SBFCs and provides new methodology and understanding with significant importance for both fundamental and applied R&D on new-generation fuel cell materials and technologies.

INTRODUCTION

The overuse of conventional energy sources such as coal, oil, and natural gas fossil fuels has caused many climate problems, resulting in environmental crisis and energy shortage (Fan et al., 2018). This scenario asks for sustainable energy alternatives with high efficiency and flexibility (Gao et al., 2016). Within this context, solid oxide fuel cell (SOFC) technology is an attractive candidate for energy conversion and energy management. SOFC can directly convert chemical energy including hydrocarbon fuel into electricity, accompanying high efficiency and low environmental impact in all-solid-state phases (Ormerod, 2003; Brett et al., 2008). Traditionally, an SOFC consists of three layers/components, namely anode, electrolyte, and cathode (Figure 1A), in which the electrolyte plays an important role (Stambouli and Traversa, 2002). Typically, the electrolyte is a pure ionic conductor, which is responsible for ionic transport and further prevents the device from electronic short circuit (Winter and Brodd, 2004). Ionic transport also supports cell redox reactions of hydrogen oxidation reaction (HOR) and oxygen reduction reaction (ORR). However, the sufficient ionic conductivity (0.01–0.1 S cm^{-1}) of electrolytes such as yttria-stabilized zirconia (YSZ) may be achieved at high temperature (800°C–1000°C), raising the cost of SOFC implementation and hence hindering its commercialization (Wachsman and Lee, 2011; Gao et al., 2016).

Many efforts have been dedicated to reducing the operating temperature of SOFCs by developing alternative materials and technologies (Shao and Haile, 2004; Huang et al., 2006; Wang et al., 2008; Ma et al., 2010; Fan et al., 2013; Fan et al., 2014; Boldrin and Brandon, 2019; Joo et al., 2019; Ding et al., 2020; Fop et al., 2020). Up to date, the state-of-the-art SOFC material system is Ni-based cermet anode, YSZ electrolyte, and (La, Sr)MnO_3 cathode catalyst. The development of new electrolytes with improved ionic conductivity has been largely pursued. However, none of them can meet the rigorous requirements of YSZ in the severe condition of SOFC. Either mechanical or chemical stability or fabrication parameter can be fully ensured. Taking the $La_{0.9}Sr_{0.1}Ga_{0.8}Mg_{0.2}O_{2.85}$ as an example, it has shown the most promising characteristics to replace YSZ due to the high ionic conductivity, high electrolyte domain at the wide temperature and oxygen partial pressure, and mechanical durability (Huang et al., 1998). However, it suffers from high reactivity with the common electrode materials (Huang et al., 1999), whereas for doped ceria electrolyte, it has high ionic conductivity and intrinsic electrocatalytic activity (Steele,

[1]Jiangsu Provincial Key Laboratory of Solar Energy Science and Technology/Energy Storage Joint Research Center, School of Energy & Environment, Southeast University, Nanjing 210096, China

[2]Department of New Energy Science and Technology, College of Chemistry and Environmental Engineering, Shenzhen University, Shenzhen 518060, Guangdong Province, China

[3]Department of Chemistry, Division for Pure and Applied Biochemistry, Lund University, Naturvetarvägen 14, 22362 Lund, Sweden

[4]Department of Physics, COMSATS Institute of Information Technology, Lahore 54000, Pakistan

[5]Department of Chemical and Biological Engineering, Chalmers University of technology, Kemigarden 4, S-41296 Goteborg, Sweden

[6]Department of Aero & Auto Engineering, Loughborough University, Loughborough LE11 3TU, UK

*Correspondence: fanld@szu.edu.cn (L.F.), rizwanraza@cuilahore.edu.pk (R.R.), j.Kim@lboro.ac.uk (J.-S.K.), zhu-bin@seu.edu.cn (B.Z.)

https://doi.org/10.1016/j.isci.2021.102191

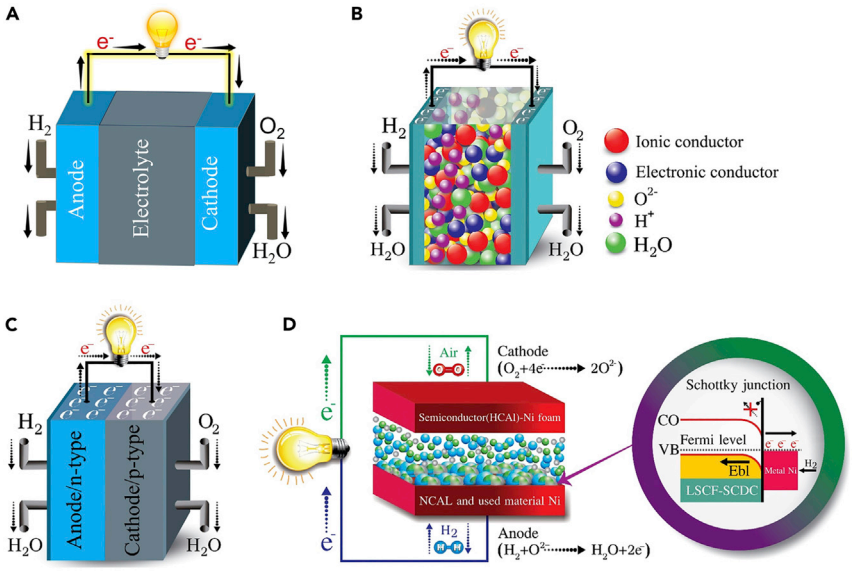

Figure 1. Structures of typical fuel cell devices

Schematic presentation of different kinds of fuel cell technology: (A) SOFC; (B) SLFC; (C) DLFC; (D) Schottky junction (SJ)-based fuel cell (Wu et al., 2020).

2000). The electronic conduction at the reduced oxygen partial pressure and low mechanical strength (Tuller and Nowick, 1977; Navarro et al., 1997; Mogensen et al., 2000; Shen et al., 2014) results in low electrical energy conversion and Faraday effiency, making it hard to completely replace YSZ for commercial application. Recently, the usage of proton-conducting ceramic fuel cells (PCFCs) may be highlighted as a suitable new trend to the above-mentioned challenge operated at intermediate temperatures (Fabbri et al., 2010b; Duan et al., 2015; An et al., 2018; Choi et al., 2018; Duan et al., 2019; Serra, 2019; Duan et al., 2020). However, currently used $BaZrO_3$- or $BaCeO_3$-based electrolytes in PCFCs were discovered 40 years ago by Iwahara et al. (Iwahara et al., 1981); the available proton (H^+) conductivity is far lower than 0.1 S cm^{-1} at 600°C (Kreuer, 2003; Fabbri et al., 2010b; Duan et al., 2015). Over a course of time, the lack of high ionic conductivity of electrolytes has been a significant challenge in complex three-layer anode/electrolyte/cathode construction with a targeting operational temperature $\leq$600°C. In addition, the anode/electrolyte and electrolyte/cathode interfaces can cause serious interfacial polarization, resulting in significant power losses for the entire fuel cell devices (Steele and Heinzel, 2001; Wilson et al., 2006).

In the development of novel materials, since 2011, many groups have utilized semiconductor heterostructure composites as an effective approach for the development of superionic conductors to reach desired ionic conductivity (>0.1 S cm^{-1}) at low temperatures (<550°C) (Zhu et al., 2011a; Zhu et al., 2011c; Liu et al., 2012; Xia et al., 2012; Dong et al., 2014; Lan and Tao, 2014b; Li et al., 2016; Asghar et al., 2018). In the initial research, Zhu et al. (Zhu et al., 2011c; Liu et al., 2012) introduced single-layer fuel cells (SLFC, Figure 1B) based on the physical configuration of the cell and then proposed double-layer fuel cell (DLFC, Figure 1C) devices without using a physically separated electrolyte layer (Zhu et al., 2011c), and that is also named as a semiconductor-based fuel cell (SBFC) based on the phenomenon the cell developed. SLFC is constructed simply by one homogeneous functioning layer, which is formed by mixing semiconductor (usually consisting of n and p-type) with an ionic conductor, as shown in Figure 1B. In parallel, DLFC is a derivative structure of SLFC constructed by using two typical components in SOFC, anode and cathode. It has been reported in the literature that both cells could function precisely like conventional three-component SOFCs (Zhu et al., 2013; Zhu et al., 2015; Zhu et al., 2017). Compared with the traditional three-layer fuel cell devices (He et al., 2000a; Wilson et al., 2006), these new SBFC devices have shown intriguing advantages (Lu et al., 2016; Fan et al., 2018), such as (1) simplicity and affordability, because less raw material and fabrication and production line are required; (2) compatibility, as the issues with the chemical/thermal/mechanical incompatibility among cell components are significantly reduced; and (3) increased effectiveness considering the two electrode/electrolyte interfacial polarization resistances are eliminated, which make up the major voltage loss

in SOFCs. All these advantages contribute to a low-cost, highly efficient, and harmonious and reliable energy conversion from chemical energy to electricity.

It should be noticed that some of the commonly used cathode materials, e.g., perovskite oxides for SOFCs, possess amphoteric property, i.e., in anode environment, showing n-type and in cathodic one as p-type properties, which can be used for the anode (Singh et al., 2013; Su et al., 2015). Therefore, the fuel cell can not only be constructed as above-mentioned DLFC but also by using one SOFC cathode component with a Schottky junction (SJ) type, as shown in Figure 1D (Zhu et al., 2015). In SJ-based fuel cells, an anode catalyst such as transition metal (Ni/Co) oxide metal is reduced when operated under fuel cell to form an SJ contact with a semiconductor component (usually a cathode mixed with electrolyte), thus preventing the electron from crossing over the device. The SJ-based fuel cells are also an SLFC-like device.

As an SLFC-like example, strongly correlated semiconducting perovskite oxide to proton conductor has been reported (Zhou et al., 2016; Lu et al., 2020). Zhou et al. (Zhou et al., 2016) reported that the metallic conductive $SmNiO_3$(SNO) thin film was turned into a proton conductive electrolyte material for low-temperature PCFC. It has been well documented that the strongly correlated electron system enables the suppression of electronic conduction through proton-incorporation-induced Mott transition. Moreover, the proton conductivity is better than other oxygen ion or proton conductors, which suggests an alternative strategy to design emergent electrolytes for low-temperature SOFCs/PCFCs. The correlated electrons and states confined to super proton conduction have also been found in fluorite structure ceria material (Xing et al., 2019). The CeO_2 surface is a nonstoichiometric $CeO_{2-\delta}$ forming as a CeO_2 core-$CeO_{2-\delta}$ shell homojunction structure between the intrinsic CeO_2 and n-type $CeO_{2-\delta}$. Such unique structure and electron states confine protons in the shell region forming super proton shuttles, leading to excellent proton conductivity of almost one order of magnitude higher than that of SNO and other proton ceramic conductors. Such core-shell homojunction structures have also been observed in perovskite semiconductors, such as $SrTiO_3$ and La-doped $SrTiO_3$ (Chen et al., 2018; Chen et al., 2019). These works shed light on a general methodology to develop distinctive interfacial structures and properties using semiconductor heterostructures. The semiconductor heterostructures have been widely applied as novel SBFCs (Zhu et al., 2011a; Zhu et al., 2011c; Zhu et al., 2013; Dong et al., 2014; Zhu et al., 2015; Zhu et al., 2016b; Shao et al., 2019; Xia et al., 2019).

As demonstrated, a novel SBFC can realize the same function as traditional electrolyte-based fuel cells for fuel-to-electricity conversion. In the SBFCs, there is no traditional ion-electrolyte layer. Typically, a semiconductor-ionic membrane is employed, which possesses the same function for the O^{2-} and H^+ transport. Generally, in the hybrid H^+/O^{2-} ionic conductor case, H^+ and O^{2-} can meet directly in the fuel cell process to generate water and electricity; the working principle of this SBFC can be presented as follows:

On the hydrogen contact side:

$$H_2 \rightarrow 2H^+ + 2e^- \quad \text{(Equation 1)}$$

On the air contact side:

$$\frac{1}{2}O_2 + 2e^- \rightarrow O^{2-} \quad \text{(Equation 2)}$$

The redox reaction is completed with

$$2H^+ + O^{2-} \rightarrow H_2O \quad \text{(Equation 3)}$$

In H^+ transporting case, H^+ can meet O_2 in the air-contacting side to generate water.

On the hydrogen side:

$$H_2 \rightarrow 2H^+ + 2e^- \quad \text{(Equation 4)}$$

On the air side:

$$\frac{1}{2}O_2 + 2H^+ + 2e^- \rightarrow H_2O \quad \text{(Equation 5)}$$

In O^{2-} transporting case, O^{2-} can meet H_2 in the hydrogen-contacting side to generate water.

On the hydrogen side:

$$H_2 + O^{2-} \rightarrow H_2O + 2e^- \quad \text{(Equation 6)}$$

On the air side:

$$\frac{1}{2}O_2 + 2e^- \rightarrow O^{2-} \quad \text{(Equation 7)}$$

Nevertheless, the overall fuel cell reaction is

$$H_2 + \frac{1}{2}O_2 \rightarrow H_2O \quad \text{(Equation 8)}$$

which is the same in all the above cases as the conventional fuel cell (Zhu et al., 2013; Lu et al., 2016). However, ionic conduction and electronic conduction co-exist in the electrolyte part at the same time of SBFCs (Lu et al., 2016). Notably, the semiconductor-ion material (SIM) can also be considered as an SOFC composite cathode component, where a cathode with p-type conducting property (e.g., typical a perovskite oxide) is mixed with the electrolyte, to acquire both electronic and ionic conduction (Kamran et al., 2019). Whereas SBFCs have already exhibited better output performances compared with the traditional electrolyte-based fuel cells from OCV (open circuit voltage) values and power output (Zhu et al., 2011a; Zhu et al., 2011b; Zhu et al., 2012; Zhu et al., 2015), thus indicating no presence of parasitic leakage or short-circuit phenomenon. The phenomenon cannot be explained by the existing fuel cell knowledge. So new working principles, semiconductor junction principles, have been naturally applied to enhance scientific understanding. For example, the bulk p-n heterojunction, planar p-n heterojunctions, and SJ have been introduced respectively to relevant SBFC devices (Zhu et al., 2011c; Zhu et al., 2015). SBFCs are good examples to further develop both the science of physics and the electrochemical properties of fuel cells, exhibiting promising technologies for applications (Zhu et al., 2012; Zhu et al., 2013; Zhu et al., 2015). It may be highlighted that the classic electrolyte layer, as the core component of fuel cells, is not indispensable although it has been used over the past 180 years since Grove invented the first fuel cell in 1839 (Zhu et al., 2011c; Singh et al., 2013), which, however, can be transformationally replaced through semiconductors and resulted heterostructures, named as SBFCs.

Based on intensive developments of functional semiconductor materials and device technologies, as well as the principle understandings in the last 10 years, firstly, we present a new perspective on fuel cell devices from semiconductor physics for better understanding its new scientific principles and highlight a new way to realize its energy conversion process. Then, we give an overview of the electrochemical processes taking place in SBFCs, which proves the SBFCs do the same electrochemical fuel-to-electricity as for the standard fuel cells while addressing the issue of the electronic short-circuit following a massive review on various SBFCs with different heterojunctions. Finally, an outlook for future development and challenge is presented by introducing new designing methodologies of energy band, interfacial superionic conduction, and built-in electric field (BIEF) assisting ionic transport and enhancement of the device performance; all these are beyond conventional fuel cell science and technology.

A NEW PERSPECTIVE ON FUEL CELL DEVICE FROM SEMICONDUCTOR PHYSICS

In 2013, Singh et al. (Singh et al., 2013) presented a new aspect to fuel cell from physics, where anode and cathode are recognized as n- and p-type regimes, respectively, which are separated by an ionic conducting electrolyte. The electrolyte is the core component of the fuel cell. As shown in Figure 2A, the SOFC is constructed by the amphoteric oxide semiconductor anode and cathode and the ionic electrolyte, where n- and p-type regimes correspond to anode and cathode in different oxygen partial pressures. In this regard, the fuel cell components can also be further defined from semiconductor physics aspects (Singh et al., 2013). The ionic electrolyte materials show similar properties/behavior as intrinsic semiconductors with a larger bandgap value over common semiconductors (Asghar et al., 2018). For example, the bandgap of state-of-the-art electrolyte yttria-stabilized zirconia is 5.79 eV (Götsch et al., 2018), which has resulted in a very low electronic conductivity. Whereas the anode and cathode, located in reducing and oxidizing atmosphere respectively responsible for HOR and ORR, should at least possess high electronic/hole conductivities (Adler, 2004). Therefore, they require low bandgap materials to enable sufficient n-type and p-type conduction. A typical example is the perovskite oxide electrode, a typical family material possessing mixed ionic and electronic/hole conductivity (Sunarso et al., 2017; Sun et al., 2020). In particular, many redox-stable perovskite oxides show amphoteric oxide properties depending on the applied atmosphere, which

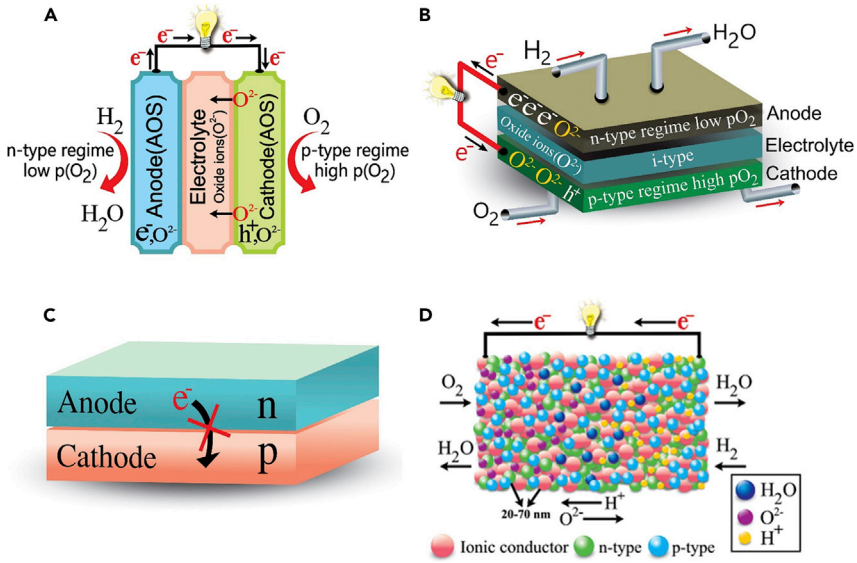

Figure 2. Fuel cells from semiconductor physics perspective

(A–C) Schematic illustration of (A) an SOFC (AOS represents amphoteric oxide semiconductor). Redrawn with permission (Singh et al., 2013). Copyright 2013, Royal Society of Chemistry. (B) A p-i-n fuel cell device and (C) a p–n junction device assembly with electrolyte free layer.

(D) SBFC device. Redrawn with permission (Asghar et al., 2018). Copyright 2018, Elsevier.

have been demonstrated using the same material for anode and cathode catalysts in symmetric SOFCs (Su et al., 2015). The symmetric configuration significantly reduces material and fabrication investment, whereas it improves anti-poisoning capability and durability.

To summarize, from the semiconductor aspect, the fuel cell may be represented as a semiconductor p-i-n three-layer device using respective n-type anode, intrinsic type electrolyte (no or very less electronic conduction compared with the ionic one), and p-type cathode, as shown in Figure 2B. This type of device is very similar to the one in solar cell devices (Liu and Kelly, 2014; Oikawa et al., 2015; Wu et al., 2015). Furthermore, if the middle electrolyte layer (i-type) is removed, a p-n two-component/layer device, i.e., DLFC, naturally appears, which is a p-n heterojunction device (Figure 2C). There is no doubt such a p-n junction device works well in the solar cell without an electronic short circuit, so do the same for the fuel cell. The p-n junctions including bulk p-n heterojunction materials, i.e., one SLFC consisting of p- and n-type semiconductors mixed with the ionic conductor, as illustrated by Figure 2D, have been widely reported for SBFCs to block electronic crossover due to the space charge region that contributes to avoiding the potential electronic short-circuit threat (Zhu et al., 2011c; Zhu et al., 2013; Zhu et al., 2016b).

It is well known that the fuel cell device can convert fuel chemical energy into electricity (Ormerod, 2003; Brett et al., 2008). The working principle of such a device lies in its ability to realize the redox reactions, i.e., HOR and ORR via charge (electron and ion) transfer processes (Winter and Brodd, 2004). This implies that, as long as a device can complete the HOR and ORR under fuel and air conditions, the fuel-to-electricity (fuel cell) can be realized. Therefore, various junctions can be applied for fuel cells as long as electrons can be prevented from passing through internal devices. The absence of the traditional ion-electrolyte separator results in the breakthrough advantage for SBFCs, as it breaks limitation by the low ionic conductivity of the electrolyte, which is a major challenge over a long historical period faced by the fuel cell technology (Sata et al., 2000; Wilson et al., 2006; Wachsman and Lee, 2011; Gao et al., 2016). The semiconductor and heterostructures, working as a functional layer to replace the conventional electrolyte for SOFC/PCFC, cannot be understood and accepted according to traditional fuel cell science and technology because electronic conduction-accompanied semiconductor is expected to cause the short circuit, resulting in losses for voltage and fuel cell efficiency. In addition, various semiconductors and heterostructure materials have been demonstrated with their capacity of higher ionic conductivity and fuel cell performance, whereas the new science behind is worthy of reviewing. Therefore, as a new research field, a complete review of the current research advance from the material and structure, especially from the junction and energy band/alignment aspect has been introduced to explain

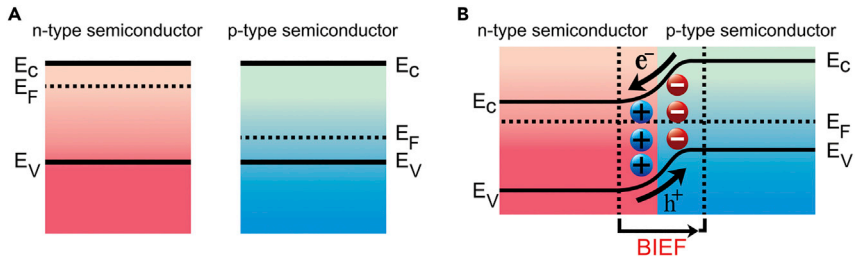

Figure 3. Energy band structure for p-n junction

Schematic of (A) energy band of n- and p-type semiconductor before contact and (B) energy band bending when p-n heterojunction is formed after contact.

the avoiding of electronic short-circuit issues and the improvement of ionic conductivity and fuel cell performance in SBFCs. There are limited review works on the material advances for SBFCs (Lu et al., 2016; Fan et al., 2018), as the key points of SBFCs, the working principle, or non-short-circuit behavior reserves for particular input, because the conventional concept does not explain what has been monitored. Therefore, the focus of this work is given to junction type, their corresponding energy band/alignment, and the local BIEF information and consequently fuel cell functionality and electrical performance. The discussion of the principle or electrochemical process will be of great interest for fuel cell communities to develop new fuel cells based on semiconductors and semiconductor (band)-electrochemistry principle, and it may influence other research fields, especially in energy conversion and storage fields, like photo-voltaic/catalysis and metal-air batteries, as further semiconductor and cell components with distinct individual principles are discovered.

COMPARISON BETWEEN SBFCS BASED ON DIFFERENT HETEROJUNCTIONS

Heterojunction refers to the interaction region formed by the contact of two different semiconductors having different dominant charge carriers. Due to the diffusion of the majority charge carrier driven via concentration difference and the minority charge carrier's drift motion, the formed interaction region is defined as the space charge region, wherein exists the BIEF (Huang et al., 2018; Li et al., 2018; Zhao et al., 2020).

A typical case is the p-n heterojunction. Once p and n semiconductors are in contact, electrons diffuse from the n-type to the p-type conduction band and holes from the p-type to the n-type valence band due to the concentration difference. These processes continue until Fermi levels of the n- and p-type semiconductors are aligned, leading to the energy band bending from the p-type to the n-type, as shown in Figures 3A and 3B. Therefore, an electric field barrier is formed to prevent the further electron motion from n-type to p-type layer and hole from p to n layer until the band bending is completed. In the case of bulk p-n heterojunction, each spatial p-n heterojunction still goes through the above process, however, at the micro and particle scale (Zhang et al., 2018; Li et al., 2019). The barrier and the BIEF are important aspects of semiconductor heterojunction to block the electron transfer and enhance ionic conduction (Wang et al., 2016a; Mi et al., 2018).

The heterojunction space charge region and ion concentration potential have a synergistic effect on the charge transport in SBFCs. Hence, there exist two driving forces for ionic transport in SBFCs, one is the chemical concentration gradient and the other is the BIEF force (Ganesh et al., 2019; Mushtaq et al., 2019). In addition, SBFCs are built on the semiconductors or SIMs possessing mixed ionic and electronic conduction, which can build up the three-phase boundary (TPB) to promote the HOR and ORR processes (Meng et al., 2018; Chen et al., 2019).

Different types of semiconductor heterojunctions such as planar p-n heterojunction (Zhu et al., 2011c) and bulk p-n heterojunction (Zhu et al., 2013; Asghar et al., 2018) have been applied in SBFCs. These semiconductor heterojunctions increase the performance of SBFCs because of the reduced electrodes/electrolyte interfaces polarization and because the heterojunction space charge region with BIEF can accelerate ion transport and avoid short circuit (Zhu et al., 2016b; Zhu et al., 2017; Xia et al., 2019).

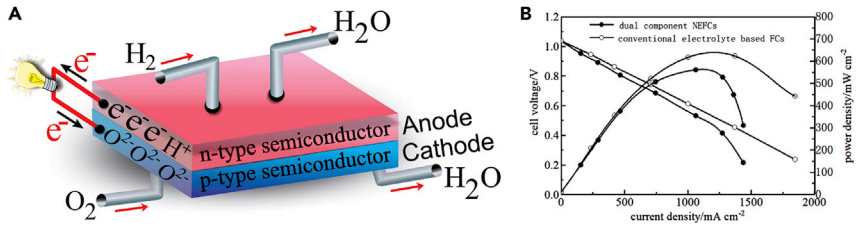

Figure 4. DLFC and its performance

(A) Schematic illustration of DLFC in case of both H^+ and O^{2-} transport and (B) its fuel cell performance compared with conventional fuel cell. Redrawn with permission (Zhu et al., 2011c). Copyright 2011, Wiley-VCH.

DLFC and planar p-n heterojunction

The DLFC was reported using an anode and a cathode analogous to the conventional SOFC (Zhu et al., 2011c) to construct SBFCs as shown in Figure 4A, which is similar to the configuration of the planar p-n heterojunction solar cells (Oikawa et al., 2015; Wu et al., 2015). Hence, we can call this anode/cathode two-layer device a planar p-n heterojunction device because the anode is n-type and the cathode is p-type. Here, a BIEF is formed directing from the anode to the cathode at the applied fuel cell atmosphere, thus avoiding the short-circuit phenomenon and simultaneously promoting the ionic conduction. It should be noticed that this DLFC was built directly using the conventional electrolyte fuel cell anode and cathode components; the results demonstrated that both conventional fuel cell and DLFC can deliver comparable power outputs (Figure 4B) (Zhu et al., 2011c).

Because anode (n) and cathode (p) possess both electron or hole with ionic conduction, only anode and cathode two-layer device can work for fuel cell function, as long as the electronic short-circuit problem is solved. This has demonstrated the above-discussed anode/cathode DLFC working principle as illustrated in Figure 2C. Furthermore, the chemical concentration difference/gradient built up at the interface between p-type and n-type semiconductors plays a significant role in the DLFC operation process (Zhu et al., 2011c; Wang et al., 2016b; Li et al., 2020). Wang et al. (Wang et al., 2016b) constructed DLFC based on the planar p-n heterojunction to further demonstrate the working principle, where a triple ($H^+/O^{2-}/e^-$) conductor $LiNi_{0.8}Co_{0.15}Al_{0.05}O_2$ (NCAL) was used as the anode layer and a mixed O^{2-} conductor $Ce_{1-x}Tb_xO_{2-\delta}$ + Co (TDC + Co), as the cathode layer. In this case, the p-type NCAL formed the planar p-n heterojunction with the n-type (TDC + Co), and the introduced depletion layer possessed a similar function to the electrolyte. At the anode side, Ni-Co can be reduced from NCAL and act as the anodic catalyst to complete the HOR reaction, which co-contributes to excellent fuel cell performance, a peak power density of 280 mW cm^{-2} at 540°C, at the reduced temperature range even with a thick device layer (1.2 mm) and without optimized catalytic activity for electrochemical reaction. It is worth mentioning that the thermal incompatibility issue of DLFCs has been much reduced compared with the conventional fuel cells when considering widely selected materials available.

SLFC and bulk p-n heterojunction

In 2000, He et al. (He et al., 2000b) reported the first-generation SLFC (Figure 5A) composed of amphoteric semiconductor materials based on Sr-doped $La_{0.9}Sr_{0.1}In_{1-y}Ca_yO_{3-\delta}$ (LSIO). LSIO possesses dominant oxygen (O^{2-}) ionic conductivity at intermediate oxygen partial pressure, whereas it becomes a p-type semiconductor under high oxygen partial pressure (e.g., in cathode environment) and n-type semiconductor characteristic at low oxygen partial pressure (anode environment). Therefore, the n-type conducting layer and p-type conducting layer are present on either side of LSIO's surface when exposed to hydrogen and air, respectively, for typical fuel cell conditions as shown in Figure 5A. In this case, LSIO between n-type and p-type layers is acting as the electrolyte and keeps its intrinsic O^{2-} ion conductivity. Therefore, such SLFC works in the same way as the conventional three-layer n-anode/electrolyte/p-cathode SOFC as well as like a p-i-n junction device. Unfortunately, the LSIO material displayed very low conductivities for O^{2-}, electron and hole; such SLFC device based on the LSIO single-layer device can deliver an extremely low maximum power density of only 3 mW cm^{-2} at 800°C, although reaching a satisfying OCV of around 1.0V. This result is too low to make an impact on SOFC society without serious attention. In 2014, Lan and Tao reported SLFC using the layered structure metal oxide, $Li_xCo_{0.5}Al_{0.5}O_2$ (LCAO), having a configuration (Lan and Tao, 2014a, 2014b): Ag/LCAO/Ag (Figure 5B). This device can also be referred to as the SLFCs. During the

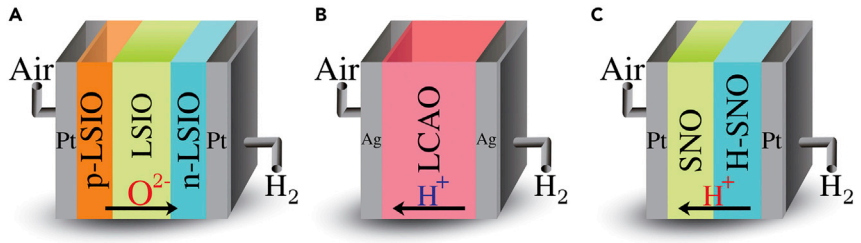

Figure 5. SLFC devices based on either ionic conductors or semiconductors

Schematic diagrams of (A) ionic electrolyte $La_{0.9}Sr_{0.1}In_{1-y}Ca_yO_3$ (LSIO), (B) SLFC with the semiconductor $Li_xCo_{0.5}Al_{0.5}O_2$ (LCAO) as the electrolyte, and (C) SLFC constructed by the semiconductor $SmNiO_3$ (SNO).

fuel cell operation, protons can be incorporated into the interlayer space of the LCAO-layered structure, thus tuning the LCAO semiconductor property to a proton-conducting electrolyte. Interestingly, this type of SLFC reached a much higher power output, 173 mW cm^{-2} at 525°C. Alternatively, in 2016, SNO, a rare-earth nickelate with the perovskite structure (ABO_3) was reported as an SLFC in a configuration of Pt/SNO/Pt (Figure 5C) (Zhou et al., 2016). Similar to LCAO, the SNO can turn to a proton conductor via a Mott-transition in *in situ* operation, where a hydrogenated H-SNO was proposed to form a bilayer structure of SNO/H-SNO. This is also an example of SLFC. With 5% H_2 in argon as fuel and air as the oxidant, the SNO device delivered 225 mW/cm^2 with an OCV around 1.0 V at 500°C. As illustrated in Figure 5C, the thin H-SNO layer is formed in the fuel cell environment attached to the SNO bulk in the device.

The above-described SLFCs based on either O^{2-} ion or H^+ conductor and semiconductor properties are finally turned to work in the same way as the conventional SOFC. The SIMs with high catalytic activity toward electrode reactions can have comparable electrochemical performances in the fuel cell device (Fan et al., 2012; Hu et al., 2015b; Zhu et al., 2016b; Zhu et al., 2017; Shao et al., 2019; Lu et al., 2020). Such performance is attributed to the proper ratios of ionic and electronic conductors (Fan et al., 2012). SLFC based on bulk heterojunction (BHJ) may have more advantages over DLFCs, because there are distinct interfaces of two p- and n-layers to cause significant interfacial polarization losses in the DLFC. Being different from the DLFC planar p-n junction constructed at the macro-component device level, the SLFC is built on the BHJ, with the p- and n-type particles distributed at the micro-particle level throughout the single-layer devices (Zhu et al., 2013). As shown in Figure 6A, the single layer is a homogeneous layer mixed with both ionic (O^{2-}/H^+) and semi- (p- and n-type) conductors, where the BHJ is formed when n- and p-type semiconductors are in contact at the particle level. Meanwhile, as seen in Figure 6B, the BIEF may be formed due to the redistribution of charges, avoiding short circuit while facilitating ion transfer. In fact, the BHJ device is ascribed to the amphoteric characteristic of metal oxide semiconductors that the direction of BIEF is generally from the fuel to air side (Singh et al., 2013). Hence, the p-n space gradient is established due to the difference in hydrogen and air (oxygen) concentrations. In this case, n-type dominates on the hydrogen side and p-type on the air side, resulting in a proper overall BIEF direction, to avoid internal electrons passage as seen in Figure 6B.

Nano-redox (HOR, ORR) is a novel concept for a fuel cell. The overall nano-redox principle is presented in Figure 6 (Zhu et al., 2013), which is determined by the reaction of ions (H^+ or O^{2-} or both). In general, both H^+ and O^{2-} may be transported to the corresponding cathode and anode side and the nano-redox reaction can take place on the surface of the nanocomposite particles, which consist of n, p, and ionic conducting particles as shown in Figure 6C.

Zhu et al. (Zhu et al., 2013) first reported such BHJ fuel cell with a homogeneous single-layer mixture consisting of metal oxides, $Li_{0.15}Ni_{0.45}Zn_{0.4}$ oxide (LNZ), and ion-doped ceria (Gd^{3+} or Sm^{3+} doped ceria, GDC, or SDC). Several reports have been released latterly to further investigate the charge separation and ion transfer mechanism through BHJ, utilizing the fabrication of the Ca^{3+} and Sm^{3+} co-doped ceria (SCDC) and perovskite structure materials such as $La_{0.6}Sr_{0.4}Co_{0.2}Fe_{0.8}O_3$ (LSCF) and $SrFe_{0.75}Ti_{0.25}O_{3-\delta}$ ($SrFe_{0.2}Ti_{0.8}O_{3-\delta}$) (Kamran et al., 2019; Mushtaq et al., 2019); especially, LSCF is a commonly used SOFC cathode material. Both BHJ-based fuel cell devices can achieve good fuel cell performance without electrochemical leakage. The charge separation and electron short-circuit mechanism have been further clarified. As shown in Figure 7A, for SDC/ZnO/NiO_x configuration, BHJ is formed in the middle region where NiO_x is a p-type semiconductor and ZnO is an n-type semiconductor. Interestingly, NiO_x can behave as

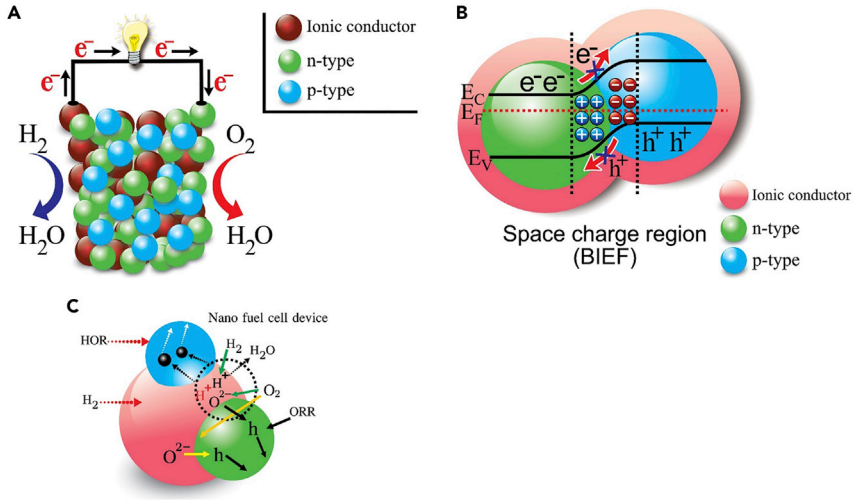

Figure 6. SLFC designed by nano-redox principle

Schematic diagram of (A) SLFC with a homogeneous layer mixing with the ionic conductor and semiconductors (n- and p-type). Redrawn with permission (Zhu et al., 2011c). Copyright 2011, Wiley-VCH, (B) bulk p-n heterojunction and the induced BIEF at the particle level in the fuel cell mode and (C) nano-redox reaction and charge transfer on the particles of ionic conductor and semiconductor (n- and p-type). Redrawn with permission (Zhu et al., 2013). Copyright 2013, Elsevier.

n-type in the H_2 atmosphere and p-type in the O_2 atmosphere. Eventually, electron transfer can take place by n-type for anode and hole transfer by p-type for the cathode. On the other hand, as can be seen in Figure 7B, for SCDC/LSCF configuration, BHJ is formed in the anode region where SCDC is an n-type semiconductor in the reduced atmosphere and LSCF is an intrinsic p-type semiconductor. The electron insulator exists in the middle part due to the intrinsic SCDC, which is an ionic conductor here, and the p-type LSCF, which does not have electron mobility. The case of BHJ at the micro-level is illustrated in Figures 7C and 7D; each spatial p-n heterojunction has the same energy band bending as the macro-double-layer p-n junction, of which the energy band bending is from the p-type semiconductor particle to the n-type one.

BHJ fuel cell devices could also be constructed using PCFC cathodes in the semiconductor heterostructures. For instance, Xia et al. (Xia et al., 2019) used a good PCFC cathode $BaCo_{0.4}Fe_{0.4}Zr_{0.1}Y_{0.1}O_3$ (BCFZY), a p-type semiconductor with the $H^+/O^{2-}/e^-$ triple-conduction, with n-type ZnO to construct a spatial BCFZY-ZnO p-n BHJ, and also the same for $SrFe_{0.2}Ti_{0.8}O_{3-\delta}$-ZnO (Kamran et al., 2019). Interestingly, such BHJ fuel cells could achieve an OCV of 1.01 V without an electronic short circuit and a peak power output of 643 mW cm^{-2} at 550°C. On the other hand, the $SrFe_{0.2}Ti_{0.8}O_{3-\delta}$ alone could also function as the electrolyte, but only reached a power density of 320 mW cm^{-2} (520°C), whereas the heterostructure composite reached a higher 650 mW cm^{-2}. All these BHJ devices have demonstrated an interface-enhanced effect, where the BIEF facilitates ionic transportation. This has the potential to lower operating temperatures without performance sacrifice due to the increased ionic conductivity and subsequently intensified the triple-phase boundary (Zhu et al., 2011c; Zhu et al., 2013; Zhu et al., 2016b). Table 1 summarizes the performances of the discussed BHJ-based fuel cells with updated most recent results. Excellent fuel cell performance, both OCV and fuel cell peak power densities at the reduced temperature over classic SOFCs, have been verified in the last 10 years with the quick deployment of new material and evolution of fuel cell fabrication technology. It should be noted that more and more work paid attention to the large cell fabrication and testing as well as operational durability of SBFCs under real cell operational conditions, which make a substantial step toward practical application.

Despite the successful fabrication and demonstration of such BHJ structure in fuel cells, there are some challenges. For instance, the materials not only have to exhibit good ionic and electronic conductivity but also require to satisfy redox stability and high catalytic activity (Wang et al., 2016b). Furthermore, BHJ needs delicate nano-engineering to customize the conductivity of p- and n-semiconductors, using heterostructure composite technology to overcome the short-circuit issue (Fan et al., 2012; Dong et al., 2014). These rigorous requirements inadvertently restrict the choice of available materials (Dong et al., 2014; Wang et al., 2016b).

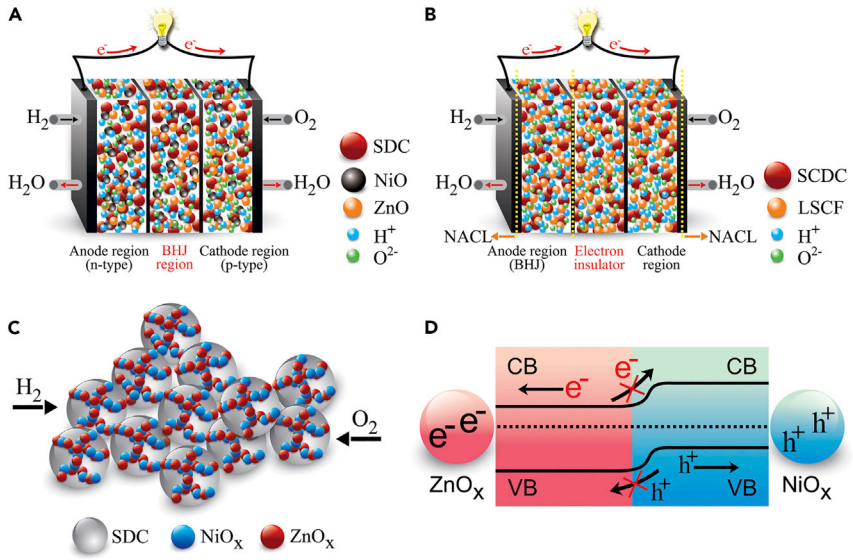

Figure 7. SBFCs based on BHJ and micro mechanism

Schematic diagram of (A) SDC/ZnO_x/NiO_x configuration, where the anode region is n-type dominated, the cathode region is p-type dominated, and BHJ is formed in the middle region. (B) SCDC/LSCF configuration; (C) BHJ network constructed by an ionic conductor (SDC) and semiconductor particles (NiO_x and ZnO). (D) The energy band structure of heterojunction produced between n- and p-type particles. Redrawn with permission (Zhu et al., 2013). Copyright 2013, Elsevier.

Schottky junction-based SBFCs

Another effective way to block the electronic conduction through the cell is to use the SJ, analogous to the functionality in solar cells (Mubeen et al., 2013; He et al., 2015; Meng et al., 2016), photocatalysis (Wang et al., 2014; Pan et al., 2020), piezoelectricity (Wang, 2010; Zhou et al., 2012; Pan et al., 2020), triboelectric nanogenerators (Wang et al., 2020), and electrocatalysis (Long et al., 2014; Aijaz et al., 2016; Xu et al., 2018). Generally, the SJ is formed when the metal and a p- or n-type semiconductor are in contact. SJ can make the fuel cell device simpler and more efficient. Figure 8A depicts the energy band of the metal and p-type semiconductor before contact. Typically, when the metal and semiconductor are in contact, the electron will transfer from the metal to the semiconductor as soon as the Fermi level of a semiconductor is lower than that of the metal (Zhang and Yates, 2012). Further as can be seen in Figure 8B, the electron flow continues until the Fermi level is aligned. The electron near the metal surface is depleted and a region defined as space charge region is consequently formed, where metal is positively charged and the semiconductor is negatively charged, near its interface. At the same time, the energy band bends upward due to the Fermi level alignment process, which acts as the Schottky barrier for blocking the further flow of electrons to the semiconductor. The Schottky barrier could be calculated as follows:

$$\varphi_{SB} = |\varphi_m - \chi_s| \quad \text{(Equation 9)}$$

where φ_{SB} is the Schottky barrier; φ_m, the work function of metal; and χ_s, the electron affinity of the semiconductor.

Moreover, the SJ can be built up *in situ* at the interface between a metal and an n- or p-type semiconductor (Zhu et al., 2015; Qiao et al., 2018). The pioneering work on a p-type SJ-based fuel cell was reported by Zhu et al. (Zhu et al., 2015) in 2015, in which the fuel cell configuration of Ni-foam/LCN ($LiNi_{0.85}Co_{0.15}O_{2-\delta}$)-NSDC ($Ce_{0.8}Sm_{0.2}O_{1.9}$-$Na_2CO_3$)/Ag was used. Unlike conventional SOFCs, where the electrolyte is used as an electron insulator, here, LCN as an intrinsic p-type semiconductor is used for heterostructure composite with NSDC. Notably, there is no short circuit observed in the LCN-based fuel cells, which attributes to the electron blocking capability of the Schottky barrier. The SJ is *in situ* formed because Ni (Co) can be formed from the reduced LCN in the anodic fuel atmosphere as shown in Figure 9A. It is also interesting to see that the replacement of cathodic Ag current collector with high conductive semiconducting metal oxide and addition of function layer of enriched LCN content at the anode side both yielded a higher SJ fuel

Table 1. A summary of performance studies of BHJ fuel cells between 2011 and 2020

Configuration	Temp. (°C)	σ_i (S cm^{-1})	σ_e (S cm^{-1})	P_{peak} (mW cm^{-2})	OCV(V)	Stability and notes	Refs
Ag/LiNiCuZn(Fe)/NKSDC/Ag	550	0.24	–	680	1.02	N/A	(Zhu et al., 2011c)
Ni-foam + LNZ/SDC + Ag	550	0.18	–	600	1.05	N/A	(Zhu et al., 2011a)
Ag/GDC-KAlZnOx/4LiNiCuZnOx/Ag	550	0.13	–	573	1.00	N/A	(Zhu et al., 2014)
Ag+6SDC/4$Li_{0.3}Ni_{0.6}Cu_{0.07}Sr_{0.03}O_2$+Ag	550	0.10	–	312	0.93	N/A	(Hu et al., 2015b)
$Li_{0.4}Mg_{0.3}Zn_{0.3}O_{2-\delta}$/$Ce_{0.9}Sm_{0.1}O_{2-\delta}$	400–600	–	–	512–250	>1.0	120 h@peak power, 15 hot/cold cycles, 6 cm*6 cm*0.1 cm large cell	(Hu et al., 2014a)
Ni/NCAL + CeO_2/$Sr_2Fe_{0.5}Mo_{0.5}O_x$ + Ni/NCAL	500–600	0.02–0.1	–	611–851	>1.0	16 h@312.5 mAcm^{-2}, 530°C	(Liu et al., 2015b)
Ni/NCAL+LSCF/SCDC + Ni/NCAL	550	–	–	1080	1.06	32 h@300 mAcm^{-2}, 530°C	(Zhu et al., 2016b)
Ni/NCAL + $LiNiFeO_2$/SDC + Ni/NCAL	550	0.26	0.14	640	1.03	10 h@680 mAcm^{-2}	(Zhu et al., 2016a)
Ni/NCAL+6LaCePrO_x/4LSCF + Ni/NCAL	550	0.07	0.001	530	0.94	14 h@0.7 V, 251 mAcm-2	(Xia et al., 2016a)
La/Pr doped CeO_2/NCAL	550	–	–	480	>1.0	70 h@380 mA cm^{-2}, cold pressing hot pressing, 6 cm*6 cm large cell	(Zheng et al., 2016)
Ni/NCAL+LSCF/SCDC + Ni/NCAL	550	0.11	0.18	1000	1.08	N/A	(Zhu et al., 2017)
NCAL+5LSCF/5SCDC + NCAL	550	NA	–	812	1.08	60 h@180 mA cm^{-2}	(Wang et al., 2017)
4$Sr_2Fe_{1.5}Mo_{0.5}O_{6-\delta}$/6$Ce_{0.8}Sm_{0.2}O_{2-\delta}$	550	–	–	841	1.1	24 h@ 156 mA cm^{-2}	(Deng et al., 2017)
LixZnO−$Sm_{0.2}Ce_{0.8}O_{2-\delta}$/$CuFeO_2$	550	0.328	0.002	775	1.04	42 h@ 80 mA cm^{-2},500°C	(Wu et al., 2018b)
NiO-YSZ-LSCF	600	0.06	0.012	628	1.11	100 h@115 mA cm^{-2}	(Cai et al., 2018)
Ni/NCAL+LNZ/GDC + Ni/NCAL	550	0.25	–	801	1.05	N/A	(Asghar et al., 2018)
Ni/NCAL + BZCFY/ZnO + Ni/NCAL	400–500	0.07–0.20		248–643	1.01–1.08	30 h@470mA cm^{-2}	(Xia et al., 2019)
Ni/NCAL + $SrFe_{0.2}Ti_{0.8}O_{3-\delta}$/ZnO + Ni/NCAL	520	0.21	0.44	650	1.06	N/A	(Kamran et al., 2019)
Ni/NCAL + $SrFe_{0.75}Ti_{0.25}O_{3-\delta}$/SDC + Ni/NCAL	520	0.11	0.12	920	1.00	N/A	(Mushtaq et al., 2019)
Ni/NCAL + PSCFN/SDC + Ni/NCAL	550–650	–	–	238	0.98	25 h@0.7 V	(Shao et al., 2019)
Ag/PSCFN/SDC/Ag				161.8		52h@0.7V	
Ni/NCAL+3LSCeCrF/7SDC + Ni/LSCeCrF	550	0.15	–	837	1.117	18 h@ 0.9 V, 234 mA cm^{-2}	(Meng et al., 2019)
Ni/NCAL+5% SCNT/SDC + Ni/**NCAL**	550	0.081		1016	>1.0	20 h@0.8 V, 100 mA cm^{-2}	(Nie et al., 2019)
Ni/**NCAL**+7SDC/3LSCu + Ni/**NCAL**	550	–	–	895	1.0	75 h@100 mA cm^{-2}	(Yuan et al., 2020b)
Ni/**NCAL**+3NSDC/LiCoCuN + Ni/**NCAL**	550	–	–	598	>1.0	9 h@210 mW cm^{-2}, 469 mA cm^{-2}	(Yang et al., 2020)
Ni/**NCAL**+7 BSCFZY/3SCDC+ Ni/NCAL	370–520	0.05–0.22		260–900	1.02–1.07	38 h@0.82 V, 120 mA cm-2	(Rauf et al., 2020)
Ni/NCAL + Ni-Zn ferrites/ SDC+Ni/NCAL	550	0.17	–	760	1.05	N/A	(Yousaf et al., 2020)

Note: PSCFN $Pr_{0.4}Sr_{0.6}Co_{0.2}Fe_{0.7}Nb_{0.1}O_{3-\delta}$; BZCFY $BaCo_{0.4}Fe_{0.4}Zr_{0.1}Y_{0.1}O_{3-\delta}$; BSCFZY $Ba_{0.5}Sr_{0.5}Co_{0.1}Fe_{0.7}Zr_{0.1}Y_{0.1}O_{3-\delta}$; LSCeCrF: $La_{0.65}Sr_{0.3}Ce_{0.05}Cr_{0.5}Fe_{0.5}O_{3-\delta}$; SCNT: $SrCo_{0.8}Nb_{0.1}Ta_{0.1}O_{3-\delta}$; LSCu: $La_{1.85}Sr_{0.15}CuO_4$; LiCoCuN:$LiCo_{0.225}Cu_{0.075}Ni_{0.7}O_{3-\delta}$.

cell performance, highlighting the positive role of SJ for charge separation and ionic conduction. On the other hand, as shown in Figures 9B and 9C, unlike the common SJ, the band bending in the SJ fuel cell device can be changed, owing to the synergy of injected H^+ concentration in the fuel cell operation, induced potential field, and the SJ BIEF, which may enhance the electron blocking effect. Here, the green section

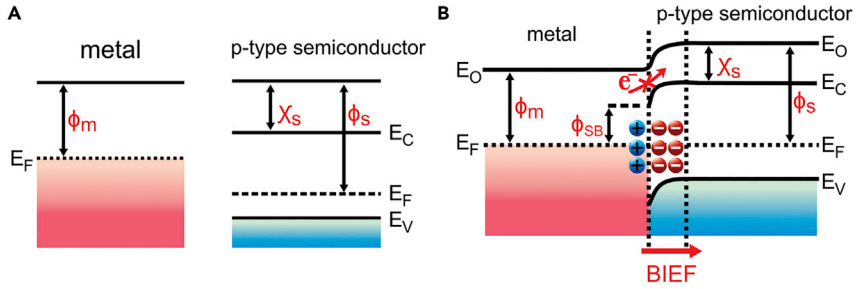

Figure 8. Energy band structure for SJ

Energy band diagram of SJ of metal and p-type semiconductor: (A) before contact and (B) after contact. E_c, the energy of minimum conduction band; Ev, the energy of maximum valence band; E_F, Fermi energy; E_0, the vacuum energy; φ_s, the work function of semiconductor; φ_{SB}, the Schottky barrier; φ_m, the work function of metal; χ_s, the electron affinity of the semiconductor.

represents the band bending on the semiconductor surface for the common SJ, which can be represented by the potential difference φ_{BB}:

$$\varphi_{BB} = |\varphi_s - \varphi_m| \quad \text{(Equation 10)}$$

The yellow section in Figure 9C represents the band bending caused by an additional H^+ concentration potential field (Zhu et al., 2015). Notably, the lower H^+ concentration, formed in the region closer to the semiconductor than that at the interface, causes a bulge of the energy band, which may also enhance the SJ barrier. Furthermore, the resulted BIEF at the interface between metal and semiconductor directs to facilitate the ion (H^+ or O^{2-} ion) transport, resulting in a higher SJ fuel cell performance.

Table 2 summarizes results for the performances of SJ-based fuel cells in recent years. The semiconductor materials such as transition metal oxide (Qiao et al., 2018) and perovskite (ABO_3 structure) (Zhu et al., 2016b) have been explored for SJ-based fuel cells due to their excellent catalytic activity and high resistance to carbon deposition, which resulted in much better electrochemical performance than that of conventional SOFCs. For instance, the peak power density >1 W cm^{-2} was obtained (Qiao et al., 2018), demonstrating the significance of this technology. Overall, the SJ-based SBFCs have broadened the functional material realm and technological simplicity, exhibiting a high potential for commercialization.

n-i type interface contact based on the core-shell heterostructure

Apart from the p-n and SJ heterojunction structures, the n-type semiconductor and its intrinsic ionic conductor behavior can also form an effective BIEF to prevent the electronic short circuit or electrochemical leakage and to facilitate the charge transfer. Wang and Xing et al. (Wang et al., 2019; Xing et al., 2019) reported the SBFC can be constructed by the same semiconductor ceria material with a core-shell structure, i.e., the $CeO_2/CeO_{2-\delta}$ core-shell structure, as illustrated in Figure 10A. Here, the surface CeO_2 can be changed by simple thermal heat treatment processes or/and with subsequently reductive hydrogen atmosphere. Hence, surface oxygen vacancy of $CeO_{2-\delta}$ is increased and its electrical properties are enhanced. The CeO_2 shell is an amorphous layer as observed from a high-resolution transmission electron microscopy image (Xing et al., 2019). The stoichiometric CeO_2 in the interior grains is an insulator, whereas the oxygen-deficient surface $CeO_{2-\delta}$ is a good electronic conductor. In this case, a BIEF directed from the core to the surface is formed between the intrinsic semiconductor CeO_2 and the n-type semiconductor $CeO_{2-\delta}$. Hence, H^+ is repelled by the BIEF and can only be transported in the channel between interfaces among core-shell $CeO_2/CeO_{2-\delta}$ particles instead of migrating from the shell/surface to the bulk, so the proton bulk infiltration/transportation is suppressed, which results in proton shuttles (Figure 10B), enabling the interfacial/surface superionic conduction rather than the bulk conduction. In addition, it should be noted that such an n-i type interface contact is itself formed, not involving any other semiconductors.

TECHNICAL AND ENGINEERING ASPECTS OF SBFCS

The majority of studies in SBFC have been focused on not only single cells that involve small cell sizes to use laboratory (powder-based) methods for single full-cell fabrication but also developments to scale up for material production and techniques for short stack including metallic bipolar plates, ceramic coatings, and scaling up the cell sizes for practically applied technologies. One of the first promising results has been achieved by M.

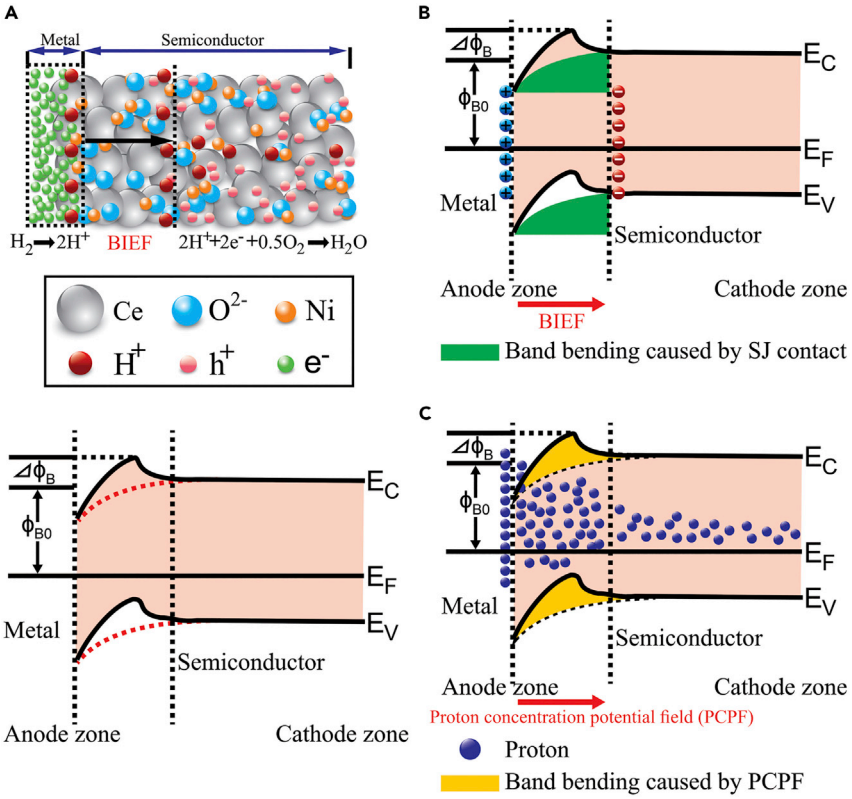

Figure 9. SBFC based on SJ and micro mechanism

Schematic diagram of (A) SJ-based fuel cell and energy band under fuel cell mode, where the H^+/e^- coupling layer exists. (B) Charge distribution and band bending caused by metal-semiconductor contact and (C) proton distribution and band bending caused by proton concentration potential field under fuel cell mode (left: initial testing and right: after proton producing). Reproduced with permission from reference (Zhu et al., 2015). Copyright 2015, Wiley-VCH.

Stingaciu et al. (Stingaciu et al., 2012) to adopt spark plasma sintering (SPS) to prepare a single cell in one single step at relatively low temperature, considering that the desired microstructure in a single-component fuel cell is quite different from that in a conventional ceramic fuel cell device. SPS is a quick, reliable, and simple technology, and it is possible to optimize the sintering parameters, such as temperature (400°C–700°C) and applied pressure (10–50 MPa), to achieve a controllable grain size and porosity. Fuel cells having a diameter of 20 mm and thickness of 0.8–1 mm with a much improved mechanical strength were prepared. A single cell with the optimized sintering parameters (550°C/25 MPa) showed a peak density of 204 mW cm^{-2} fed by methanol at the operational temperature of 550°C, which is generally comparable, or much higher, however, not the best compared with the open literature work at that time (Stingaciu et al., 2012). A lower or higher sintering temperature results in a lower fuel cell performance. Higher performance is expected to be forthcoming from SBFCs, considering the absence of conventional problems concerning electrodes, such as interface compatibility, interface resistance, or high ohmic resistance. In addition, the use of methanol in the field of fuel cell technology is also highly desirable for its renewable production, storage, and transport. More technical details can be viewed in the latest published book and a dedicated chapter (Yuan et al., 2020a).

Large cell fabrication was performed by Hu et al. (Hu et al., 2014a; Hu et al., 2014b) by the integration of the cold-pressing shaping and then hot-pressing improving the mechanical strength. A composite phase of the ionic conductor, $Mg_{0.4}Zn_{0.6}O/Ce_{0.8}Sm_{0.2}O_{2-\delta}$, and semiconductor, $Li_{0.3}Ni_{0.6}Cu_{0.07}Sr_{0.03}O_{2-\delta}$, was prepared by co-precipitation and solid-state reaction, respectively and then mixed with a weight ratio of 4:3. Green single-cell pellets with large-scale size (6 cm* 6 cm) were first pressed and shaped, then hot-pressing with 30 tons of pressure at 650°C for 120 min to form relative dense single cells, see Figure 11A. Subsequently, the copper grating and silver paste were attached as a current collector before fixed to the fuel cell testing setup. A hydrogen flowing rate at 1000 mL min^{-1} at 1 atm pressure was used. The large cells with an active area of 25 cm^2 gave OCV above 1.0 V above 400°C and a maximum power of 12.8 W at

Table 2. A summary of performance studies of SJ-based fuel cells between 2015 and 2020

Configuration	Temp. (°C)	σ_i (S cm^{-1})	σ_e (S cm^{-1})	P_{peak} (mW cm^{-2})	Ref.
Ni-foam + LCN/NSDC + NCAL	550	0.30	NA	1000	(Zhu et al., 2015)
Ni/NCAL + $Ba_{0.5}Sr_{0.5}Co_{0.8}Fe_{0.2}O_3$/SDC + Ni/NCAL	550	0.197	0.198	655	(Afzal et al., 2016)
Ni-foam + $LiNi_{0.1}Fe_{0.9}O_2$/SDC + Ag	500	0.26	0.14	640	(Zhu et al., 2016a)
Ni/NCAL + hematite/(La,Pr)CeO_2 -LSCF + Ni/NCAL	550	0.126	0.075	375	(Xia et al., 2017a)
Ni/NCAL+LSCF/SCDC + Ni/NCAL	550	0.482	0.178	814	(Wang et al., 2017)
Ni/NCAL + $La_{0.7}Sr_{0.3}Cr_{0.5}Fe_{0.5}O_3$/SDC + Ni/NCAL	550	0.287	0.392	1059	(Meng et al., 2017)
Ni/NCAL + ZnO/(La,Pr)CeO_2+Ni/NCAL	550	0.290	1.139	1055	(Qiao et al., 2018)
Ni/NCAL + ZnO/hematite + Ni/NCAL	550	0.221	0.688	580	(Wu et al., 2018a)
Ni/NCAL + $La_{0.65}Sr_{0.3}Ce_{0.05}Cr_{0.5}Fe_{0.5}O_3$/SDC + Ni/NCAL	550	0.15	0.916	837	(Meng et al., 2019)
Ni/NCAL+5$LaNiO_3$/5SDC + Ni/NCAL	530	0.203	0.541	688	(Lu et al., 2020)

600°C, corresponding to a power density of 512 mW cm^{-2}, and the cells also gave an interesting power density above 250 mW cm^{-2} at 400°C (Figure 11B). Both power outputs are technically useful with great commercialization potential. Besides, the single cells survived after interrupted testing of 8 h for each and continued 15 times. No observation of the open-circuit voltage decline and a slight reduction of peak power density (from 512 mW cm^{-2} to 450 mW cm^{-2}) were observed. This is the first reported case study of the large cell fabrication and durability of SBFC; the encouraging performance suggests the stability of applied ionic and semiconductor materials for SBFCs. There are possibilities to further improve the durability of SBFCs. One is to lower the operating temperature of SBFCs that facilitates the physical and chemical stability of electrode and ionic conductor materials as well as the interfaces under fuel cell operation. The other chance is to use the chemically stable material to replace the easily reducible material. Those are currently being pursued and verified in many laboratories (Wang et al., 2017; Shao et al., 2019). More information could be referred to Table 1 and cited references for more details.

At present, this field is still in the research stage, with constraints in terms of engineering natures and financial supports, limiting the scope of the collected data for review. However, important analysis can be performed with respect to the material and technological aspects to strengthen the viability of the system. It is also demonstrated that the application of mixed semiconductor and ionic conductor as two major phases can realize the same functionality of the entire fuel cell, obtaining higher performance than that of the classical SOFCs. Therefore, the costs for the required raw material content as well as the material and cell fabrication are much reduced. With a simple comparison, in classical SOFCs, three material fabrication lines for Ni, YSZ, and (La, Sr)MnO_3 are required, whereas only two production lines are required for SBFCs. It is also possible to bypass the material compatibility issues because the semiconductor-based membrane can be based on the electrode materials, while simultaneously increasing cell efficiency, making them applicable for industrial purposes. Another distinct characteristic is its low-temperature operation capability compared with the present state-of-the-art above 600°C or commercial systems above 700°C. The reduced operating temperature is achieved while maintaining fuel cell performance, which cannot be replicated by the conventional approach, which allows knock-on benefits in terms of low-cost interconnect and the sealant, lowering investment while maintaining better durability. Therefore, the total cost of the cell should be largely reduced, making it more competitive in the energy conversion market.

Significant low-temperature fuel cell performance has been demonstrated with various cell structures, optimized fabrication technology, and material research. However, we need to recognize that the development of SBFCs is still in the initial/infant stage. The solid cell operational principles are not yet verified. The science behind the corresponding enhancement of the ionic conduction and/or catalytic activity in SBFCs at the reduced temperature (which cannot be reached by the classic material modification method) remains being masked. For assessing suitability toward high-temperature fuel cell and industrial purposes (e.g., automobile

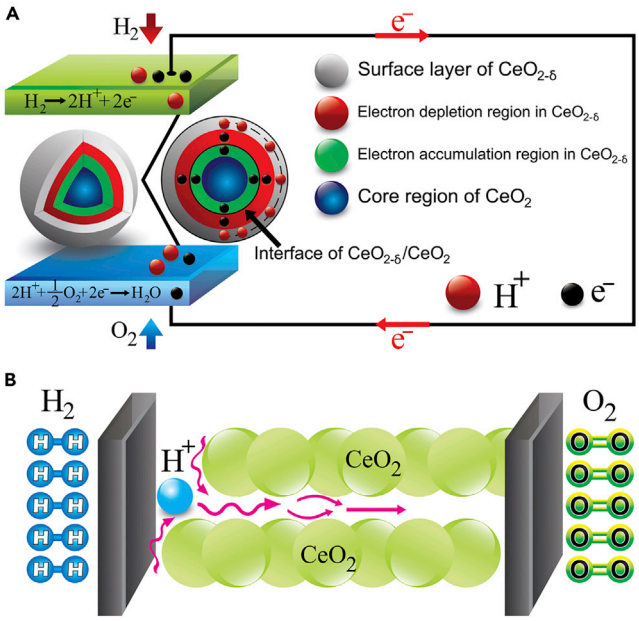

Figure 10. n-i type interface contact and "proton shuttles" transport

Schematic of (A) SBFC applying CeO_2 core-shell particles as the electrolyte and (B) the "proton shuttles" transport in the surface region of CeO_2 shell. Reproduced with permission (Xing et al., 2019). Copyright 2019, American Chemical Society.

applications for 5000 h and stationary deployment at least to 40, 000 h) operational with acceptable degradation rate should be performed; at the minimum, the durability from the accelerated testing procedure should be demonstrated. Besides, one may see that most cells are only subjected to low-temperature sintering; the mechanical strength may not be sufficient under severe fuel cell operation conditions and the possible redox cycling as well as the cool-hot cycling. However, because SBFCs integrate the low system cost and higher efficiency potential, they should deserve worldwide effort from academic researchers of various backgrounds/fields to elucidate the possible underlying science. Moreover, inputs from the industrial stakeholders and capitalist/government in the engineering and technical aspects, policy support, and cultivation are urgently required to help the technology transfer from the laboratory to the real application and to achieve its early techno-economic target for the commercialization of such novel energy conversion purposes.

COMPARISON BETWEEN SOFCS AND SBFCS

In summary, the comparisons between SOFCs and SBFCs are summarized as following from materials, technology, and costs/commercialization aspects.

Materials

As mentioned in the introduction part, SOFC is routinely composed of three-part anode electrolyte and cathode, which have taken several decades for research and development on the electrolyte and then compatible electrodes, especially on cathode materials. Basic requirements for electrolyte in SOFC are (1) sufficient oxygen ionic conductivity (0.1 S/cm) at operating temperature; (2) negligible electronic conductivity; (3) thermodynamic and chemical stability over wide range temperature; (4) compatibility with electrodes; (5) required mechanical properties etc. Representative materials are fluorite-type-based electrolytes such as ZrO_2, CeO_2, and Bi_2O_3, and perovskite-structure-based electrolyte mainly includes $LaGaO_3$, and pyrochlore-based electrolytes (Mahato et al., 2015). Although they all can be utilized as SOFC electrolytes, YSZ is nowadays the only commercial product. Its operating temperature should be 700°C–1000°C to get appreciate fuel cell performance if no thin-film technology is involved, which has been caused mainly by the high costs and complex technology.

In SBFC cases, all developed SOFC-advanced materials, especially perovskite oxide electrodes (anode and cathode), can be directly combined into SBFCs for both electrode and electrolyte membrane, so-called semiconductor-based membrane fuel cells. In this case, both electrode and membrane are based on

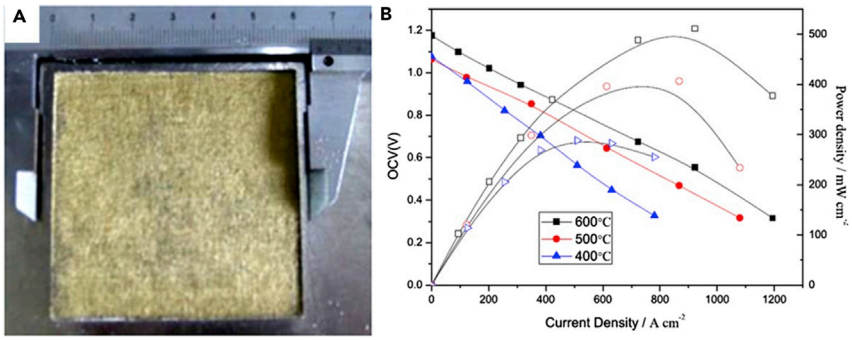

Figure 11. Large-scale SBFC device and electrochemical performance

(A) Digital picture of large-scale SBFCs in a dimension of 6*6 cm^2 (Hu et al., 2014b) and (B) electrochemical performance of resultant SBFC (Hu et al., 2014a). Reproduced with permission.

semiconductors for SBFCs have no compatible problem that has been seriously developed in decades for SOFCs, which has also made the simple SBFC technology to low-cost manufacturing. In addition, unlike the SOFC sole YSZ electrolyte that has limited flexibility of the electrode materials and high-temperature manufacturing technology, a wide range of materials are based on semiconductors (MOS: metal oxide semiconductor) such as ZnO, TiO_2, NiO, perovskite-type oxide such as $SrTiO_3$, etc. (Hu et al., 2014b; Hu et al., 2015a; Dong et al., 2016; Wu et al., 2016; Xia et al., 2016b; Zhu et al., 2016a; Cai et al., 2017; Xia et al., 2017a; Xia et al., 2017b; Chen et al., 2018; Qiao et al., 2018; Wu et al., 2018a; Dong et al., 2019; Xing et al., 2020) Especially, well-developed SOFC perovskite cathode materials, which are usually p-type semiconductors, can be used as electrolyte functions through Schottky junction principle (Zhu et al., 2013; Zhu et al., 2015; Dong et al., 2016; Zhu et al., 2016b; Zhu et al., 2017; Meng et al., 2018; Meng et al., 2019). These types of SBFCs can avoid compatibility issues between the electrolyte and electrode because the electrolyte itself contains already the electrode with good compatibility. In addition, although the semiconductor-based electrolyte possesses certain electronic conduction, the SBFC can work with even better performance as reported because of their high ionic conductivity of 0.1 S/cm in a low temperature range (<550°C) based on junction principles. Table 3 compares and summarizes the characteristics of SOFCs and SBFCs.

Technology

From a technical point of view, fabricating thin-film electrolytes for SOFC is an effective method to achieve better cells in a low-temperature range (<600°C), thus lowering the operating temperature. The most widely used techniques are pulsed laser deposition (PLD), atomic layer deposition (ALD), chemical vapor deposition (CVD), physical vapor deposition (PVD), atmospheric plasma spraying, and sol-gel (Zhang et al., 2017). However, the thin-film fabricating process is costly and complicated, in addition to a durability issue for long-life operation compared with bulk electrolyte support SOFCs. Today the reliable long-life SOFC (over 40,000 h) products are based on thick-electrolyte-supported technology such as Bloom products.

Unlike the SOFC thin-film technologies to shape the electrolyte ceramic layer to reduce the device internal resistance, the simple bulk shaping technology can be well applied for advanced SBFCs because semiconductors, e.g., SOFC perovskite cathode materials used in the electrolyte membrane, which are very similar to an SOFC cathode component without any interfacial gap problem between the SOFC electrolyte and electrode, which is a challenging technical issue to be solved in the SOFC technology because of the major power loss caused by such interfacial polarization. For SBFCs, the bulk semiconductor membrane layer as said, which can be used by SOFC a cathode component, is sandwiched between the two NCAL (or Ni-NCAL) thin electrode layers. Symmetrical electrodes are applied in the SBFC device. The cell is easy to be fabricated by normal drying powder shaping into pellet under pressure without high-temperature sintering densification process. The typical microstructures of SBFCs are shown in Figure 12 (Chen et al., 2018; Qiao et al., 2018; Chen et al., 2019; Xia et al., 2019); intrinsic semiconductor and heterostructure material layer is used as a key layer in SBFCs instead of ionic conductive electrolyte layer. The key issue different for SBFCs is low temperature (≤600°C)-treated semiconductor-based functional layer (Figures 12A and 12C), whereas the SOFC requires a dedicated high temperature (≥1300°C) multi-step co-sintering process; moreover, the SBFC can be constructed by an SOFC cathode component to realize SOFC anode/

Table 3. Comparisons between conventional SOFCs and SBFCs

Items	Complexity	Interface Loss	Driving Force	Special Features
SOFCs	Complex (three layers)	High	Chemical concentration potential difference	Electrolyte layer/separator
SBFCs	Simple (single layer)	Low	Chemical concentration potential difference and BIEF	BIEF and energy band alignment

electrolyte/cathode three-component functions and leads to simple fuel cell technology against conventional three-component ceramic shaping complex technology (Figures 12B and 12D).

Costs and commercialization

From the technical aspect, the cost for SOFC is mainly composed of fuel cell stack cost, which is influenced by many factors including material costs, machining cost, energy costs, and labor costs (Dubois et al., 2017; Harboe et al., 2020). Material costs including both SOFC and bipolar plates are made up of the main part of the total costs for the fuel cell stack. As a fact, the bipolar plates cost much higher than SOFC itself if the operational temperature is above 700°C because special and expensive alloy or ceramic bipolar plates are used. Costly thin-film technology may also be an important factor in the cost and the durability.

Challenges on SBFCs

Although there are many advantages and potentials for SBFCs, there are serious challenges toward commercialization: (1) engineering efforts are missing due to lack of corresponding financed projects, thus large area shaping SBFCs have not been carried out; (2) as a consequence, life span assessing toward commercial and industrial purposes is missing. The durability from the accelerated testing procedure should be demonstrated based on completion; (3) financial support from the industrial stakeholders and capitalist/government due to lack of public recognition on SBFCs. In a word, as pointed in the SBFCs' technical and engineering aspects, SBFCs are still in the research stage, with constraints in terms of engineering natures and efforts. Therefore, much effort is needed from the government, researchers, and industrial engineering to promote the commercialization process for SBFCs.

OUTLOOKS AND PERSPECTIVES

Design methodology of band bending/alignment for superionic conductivity at the interface

SBFCs constructed on the various junctions showed exceptional fuel cell performances over the conventional SOFCs under the same operational condition. Generally, all junction-based fuel cell devices can be explained based on energy band theory. In fact, the band alignment principle utilized in photoelectrochemical water splitting has also been successfully demonstrated in SBFCs (Dong et al., 2019). Still, precise determination and comparison of the factors that affect band bending and location are needed. Typically, in an n-type semiconductor nanoparticle, the band bending potential (V_{BB}) between distance r and particle center can be calculated as the subsequent equation (Albery, 1984):

$$V_{BB}(r) = \frac{kT}{6e}\left[\frac{r-(r_0-D)}{L_D}\right]^2\left[1+\frac{2(r_0-D)}{r}\right] \quad \text{(Equation 11)}$$

where L_D, the Debye length $L_D = (\varepsilon_r\varepsilon_0 kT/e^2N_d)^{0.5}$; D, the depletion region length; r_0, the radius of semiconductor particle; ε_r, the relative dielectric constant of the semiconductor; ε_0, the vacuum permittivity; N_d the dopant concentration. When the $r_0<\sqrt{3}D$, the Equation 11 can be simplified as (Zhang and Yates, 2012):

$$V_{BB}(r) = \frac{kT}{6e}\left(\frac{r_0}{L_D}\right)^2 = \frac{e{r_0}^2N_d}{6\varepsilon_r\varepsilon_0} \quad \text{(Equation 12)}$$

Therefore, it is important to further highlight how band bending affects fuel cell performances regarding particle size, dopant concentration, and dielectric constant of materials. Furthermore, the band bending under fuel cell mode can be fairly complicated due to the ionic potential field induced or affected by the chemical concentration differences, signifying the need for more scientific efforts to develop this field, e.g., semiconductor electrochemistry.

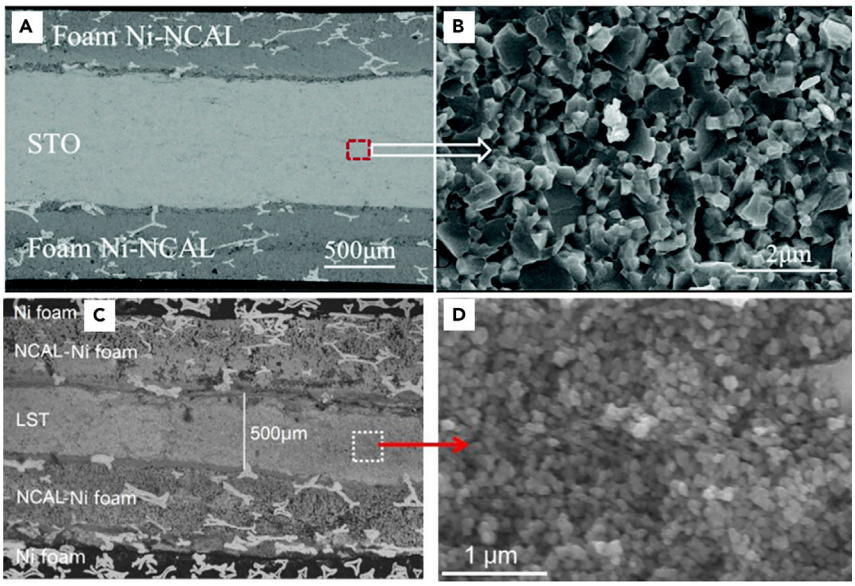

Figure 12. Typical microstructures of SBFCs

(A and B) SEM pictures for (A) cross-sectional of Ni-NCAL/$SrTiO_3$/Ni-NCAL cell and (B) magnified image of the electrolyte. Reproduced with permission from reference (Chen et al., 2019). Copyright 2019, JMCA.

(C and D) (C) SEM images of the cross-section of the symmetrical cell and (D) the magnified image of the La-$SrTiO_3$ electrolyte. Reproduced with permission from reference (Chen et al., 2018). Copyright 2018, ACS Appl. Mater. Interfaces.

Design methodology of superionic conductivity at the interface

Heterostructure interfaces play an important role in the electrochemical devices, with a particular influence on the ionic conductivity of surfaces and interfaces, in ionic solids and energy devices (Chakhalian et al., 2012; Hwang et al., 2012; Liu et al., 2015a; Zhao et al., 2020) due to the lattice mismatching, disorder, dislocation, strain, and/or space-charge formation, leading to the distinct properties as the bulk or material surface. It leads to the creation of an electric potential gradient near the surface/interface to maintain thermodynamic equilibrium, even the creation of a new phase or material state. When the space charge layer between heterostructure interfaces is on the same order of magnitude as the Debye length or if the grain size approaches the Debye length (Fabbri et al., 2010a; Seo et al., 2016), the BIEF induced by the space charge region can significantly contribute to the electric conductivity. The Debye length is determined by the dielectric constant, ionic concentration, and temperature (Despotuli et al., 2005). Here, the heterojunction interface effect on the total conductivity is observed due to the nanomaterial structure (Sata et al., 2000).

In traditional ionic principles, the heterojunction interface effect is attributed to the structural mismatch accompanying the increased defect concentration and induced stress (Fabbri et al., 2010a; Zhao et al., 2020). This is ascribed to the narrow space charge region due to heavily doped ionic conductors and the interface size much larger than the Debye length. In the case of SBFC, the BIEF induced by the space charge region may significantly promote the ionic movement because the heterostructure interface is approximately the same as the Debye length. Therefore, the BIEF electric field force and mechanical stress work together to promote ion transport, i.e., the increased ionic defects and the driving force of BIEF discussed below, forming the superionic conductive interface.

BIEF design methodology

BIEF commonly exists in different semiconductor heterostructures, as shown in Figure 13, which can be built in various material configurations of 1D nanowires (Figures 13A), 2D nano-thin films (Figure 13B), and 3D nanoparticles (Figure 13C). A more in-depth understanding of BIEF needs to be applied in fuel cells to guide developing a design methodology on new material's functionality and device performance. The semiconductor heterostructure resultant BIEF or local electric field that plays a vital role to promote ionic transfer/transport has been widely applied in batteries with implications (Xia et al., 2013; Zhu et al., 2013; Zhu et al., 2016b; Li et al., 2018). Furthermore, two impacts of the role of BIEF in fuel cell devices have been recognized: (1) to assist and promote ionic transport leading to superionic conduction in the material (Zhu

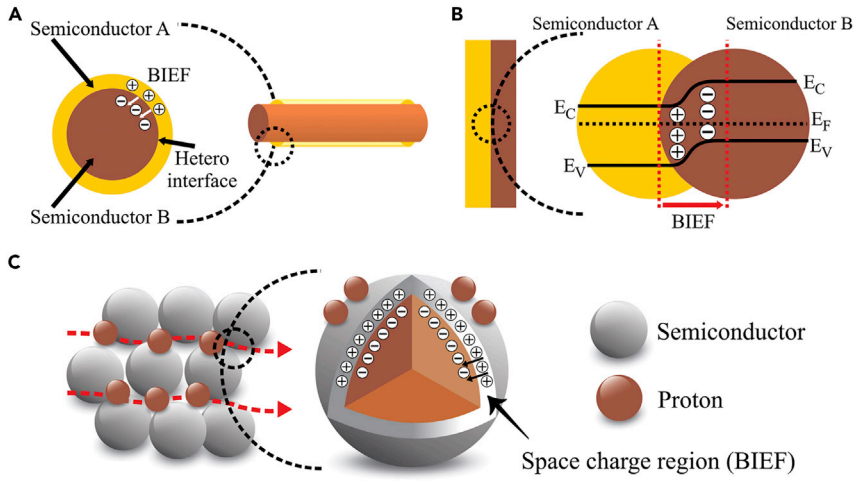

Figure 13. BIEF existing in different material configurations

Possible formation of BIEF in (A) 1D nanowire heterojunction, (B) 2D hetero-thin film, and (C) 3D nanoparticles. In the case of 3D nanoparticles, BIEF formed from the inside of particles makes the transport of ions only between particle interfaces or surfaces (Xing et al., 2019).

et al., 2013; Mushtaq et al., 2019; Xing et al., 2019); (2) to improve the durability and stability of the device (Li et al., 2018). Both benefit the high fuel cell energy conversion efficiency and durability at the reduced temperature and promote the market acceptability.

In conductive materials, the electrical conductivity can be expressed by Arrhenius relation:

$$\sigma\ T = \sigma_0\ exp\left(-\frac{E_a}{KT}\right) \qquad \text{(Equation 13)}$$

where σ is the electrical conductivity, σ_0, a pre-exponential factor, T, the thermodynamic temperature, and E_a, the activation energy of conduction. The activation energy of the ion migration is the sum of the structural association energy (E_A) and the migration energy (E_m):

$$E_a = E_A + E_m \qquad \text{(Equation 14)}$$

The E_A reflects the mobile ion to break the bond energy (Inaba and Tagawa, 1996; Jaiswal et al., 2019). Further studies reveal three remarkable effects of the BIEF on the SBFCs such as (1) the strong BIEF (10^{6-8} V/m) (Grandjean et al., 1999) to stimulate ions from static to mobile state, thus no energy needs to break the bond especially when the ions at interfaces with weak structural bonding. This means E_A is eliminated, thus the mobile ions have distinct lower activation energy for migration; (2) because of the strong BIEF, more ions can be stimulated, thus largely increase the mobile ions concentration; and (3) to add additional driving force on mobile ions' transport, i.e., enhance ionic mobility. These three effects to reduce largely ionic transport activation energy, increase mobile ion concentration, and promote ionic transport make BIEF a powerful material methodology. For example, from the Arrhenius relation, Equation 12, removing structural activation energy, the conductivity is enhanced immediately by a factor of Exp(E_A/kT). In addition, the pre-exponential factor σ_0 is related to mobile ion concentration, so enhanced conductivity is proportional to increased mobile ions activated by BIEF.

Moreover, the BIEF can directly drive the ions' transport aside from the chemical potential of ion concentration diffusion (Xia et al., 2013; Xing et al., 2019). Figure 13C allows us to estimate the BIEF direction from the n-type semiconductor particle to the p-type particle, due to the charge redistribution in the space charge region. Here, both H^+ and O^{2-} ions are driven by the induced BIEF. Especially in the case of BHJ, the accelerated ionic transport is at the particle level, where the space charge region is formed by each spatial heterojunction, which approaches the Debye length to make the BIEF effect effectively.

Based on the analysis of BIEF applied in fuel cells, a new mathematical model could be further established in the BIEF designing methodology to describe ions transport in the space charge region where the BIEF

exists. The function of current density j can be established by both the chemical potential driving force and electric driving force (O'Hayre et al., 2016):

$$j = -\frac{\sigma}{|Z_i|F}\frac{d(V_1+V_2)}{dx} - D\frac{dc}{dx} \quad \text{(Equation 15)}$$

where D is the coefficient of diffusion; c, the ion concentration; Z_i, the effective charge of the ion; F, Faraday constant, approximately 96,500 C/mol; V_1, the electrical potential due to the process of ion depletion and accumulation; and V_2, the electrical potential due to the BIEF.

Consequently, the gradient of the BIEF electrical potential (V_2) contributes to the current density, which also reflects the driving force of BIEF on the charge carrier.

The ionic conductivity σ_i can also be calculated from the following equation (Zhu, 2009):

$$\sigma_i = D\frac{c_i\,(Z_iF)^2}{KT} \quad \text{(Equation 16)}$$

where c_i is the concentration of mobile ions. Hence, the ionic conductivity is enhanced due to the increased c_i, which is attributed to the BIEF motivation for more mobile ions. Moreover, the movement rate r of ions in the electric field can be described with ionic mobility u, which represents the migration rate of ions at a unit electric potential gradient.

$$r = u\frac{dV}{dx} \quad \text{(Equation 17)}$$

where the BIEF electric potential further promotes the ion movement. Based on the above discussion, the designing methodology of BIEF is the essential and unique characteristic for the SBFCs. The electron distribution, ionic defects, and different band structures should be combined to consider the BIEF designing methodology comprehensively. The BIEF may be developed as a new robust methodology for material functionalities and device performances.

ACKNOWLEDGMENTS

This work is supported by the National Science Foundation of China (No. 51772080 and 51402093), Brain Pool fellowship program, the Research Grant for Scientific Platform and Project of Guangdong Provincial Education office (2019KTSCX151), Shenzhen Government's Plan of Science and Technology (JCYJ20180305125247308), and Natural Science Foundation of Guangdong Province (2017A030313289).

AUTHOR CONTRIBUTIONS

Enyi Hu, Zheng Jiang, Liangdong Fan, and Manish Singh contributed equally to this work, wrote and revised the paper with the assistance of all the authors. Bin Zhu and Liangdong Fan conceived the idea and oversaw the project. Rizwan Raza and Muhammad Sajid re-drew and arranged all the figures. Rizwan Raza and Jung-Sik Kim gave support and also helped to revise the paper. All authors discussed the results and contributed to the manuscript.

DECLARATION OF INTERESTS

The authors declare no competing interests.

REFERENCES

Adler, S.B. (2004). Factors governing oxygen reduction in solid oxide fuel cell cathodes. Chem. Rev. *104*, 4791–4843.

Afzal, M., Saleemi, M., Wang, B., Xia, C., Zhang, W., He, Y., Jayasuriya, J., and Zhu, B. (2016). Fabrication of novel electrolyte-layer free fuel cell with semi-ionic conductor (Ba0.5Sr0.5Co0.8Fe0.2O3−δ- Sm0.2Ce0.8O1.9) and Schottky barrier. J. Power Sources *328*, 136–142.

Aijaz, A., Masa, J., Rösler, C., Xia, W., Weide, P., Botz, A.J.R., Fischer, R.A., Schuhmann, W., and Muhler, M. (2016). Co@Co3O4 encapsulated in carbon nanotube-grafted nitrogen-doped carbon polyhedra as an advanced bifunctional oxygen electrode. Angew. Chem. Int. Ed. *55*, 4087–4091.

Albery, W.J. (1984). The transport and kinetics of photogenerated carriers in colloidal semiconductor electrode particles. J. Electrochem. Soc. *131*, 315.

An, H., Lee, H.-W., Kim, B.-K., Son, J.-W., Yoon, K.J., Kim, H., Shin, D., Ji, H.-I., and Lee, J.-H. (2018). A 5 × 5 cm2 protonic ceramic fuel cell with a power density of 1.3 W cm–2 at 600 °C. Nat. Energy *3*, 870–875.

Asghar, M.I., Jouttijärvi, S., Jokiranta, R., Valtavirta, A.-M., and Lund, P.D. (2018). Wide bandgap oxides for low-temperature single-layered nanocomposite fuel cell. Nano Energy *53*, 391–397.

Boldrin, P., and Brandon, N.P. (2019). Progress and outlook for solid oxide fuel cells for transportation applications. Nat. Catal. *2*, 571–577.

Brett, D., Atkinson, A., Brandon, N., and Skinner, S. (2008). Intermediate temperature solid oxide fuel cells. Chem. Soc. Rev. *37*, 1568–1578.

Cai, Y., Wang, B., Wang, Y., Xia, C., Qiao, J., van Aken, P.A., Zhu, B., and Lund, P. (2018). Validating the technological feasibility of yttria-stabilized zirconia-based semiconducting-ionic composite in intermediate-temperature solid oxide fuel cells. J. Power Sources *384*, 318–327.

Cai, Y., Xia, C., Wang, B., Zhang, W., Wang, Y., and Zhu, B. (2017). Bioderived calcite as electrolyte for solid oxide fuel cells: a strategy toward utilization of waste shells. ACS Sustain. Chem. Eng. *5*, 10387–10395.

Chakhalian, J., Millis, A.J., and Rondinelli, J. (2012). Whither the oxide interface. Nat. Mater. *11*, 92–94.

Chen, G., Liu, H., He, Y., Zhang, L., Asghar, M.I., Geng, S., and Lund, P.D. (2019). Electrochemical mechanisms of an advanced low-temperature fuel cell with a SrTiO3 electrolyte. J. Mater. Chem. A *7*, 9638–9645.

Chen, G., Zhu, B., Deng, H., Luo, Y., Sun, W., Liu, H., Zhang, W., Wang, X., Qian, Y., and Hu, X. (2018). Advanced fuel cell based on perovskite La-SrTiO3 semiconductor as the electrolyte with superoxide-ion conduction. ACS Appl. Mater. Interfaces *10*, 33179–33186.

Choi, S., Kucharczyk, C.J., Liang, Y.G., Zhang, X.H., Takeuchi, I., Ji, H.I., and Haile, S.M. (2018). Exceptional power density and stability at intermediate temperatures in protonic ceramic fuel cells. Nat. Energy *3*, 202–210.

Deng, H., Feng, C., Zhang, W., Mi, Y., Wang, X., Dong, W., Wang, B., and Zhu, B. (2017). The electrolyte-layer free fuel cell using a semiconductor-ionic Sr2Fe1.5Mo0.5O6-δ – Ce0.8Sm0.2O2-δ composite functional membrane. Int. J. Hydrogen Energy *42*, 25001–25007.

Despotuli, A.L., Andreeva, A.V., and Rambabu, B. (2005). Nanoionics of advanced superionic conductors. Ionics *11*, 306–314.

Ding, H., Wu, W., Jiang, C., Ding, Y., Bian, W., Hu, B., Singh, P., Orme, C.J., Wang, L., and Zhang, Y. (2020). Self-sustainable protonic ceramic electrochemical cells using a triple conducting electrode for hydrogen and power production. Nat. Commun. *11*, 1907.

Dong, W., Tong, Y., Zhu, B., Xiao, H., Wei, L., Huang, C., Wang, B., Wang, X., Kim, J.-S., and Wang, H. (2019). Semiconductor TiO2 thin film as an electrolyte for fuel cells. J. Mater. Chem. A *7*, 16728–16734.

Dong, W., Yaqub, A., Janjua, N.K., Raza, R., Afzal, M., and Zhu, B. (2016). All in one multifunctional perovskite material for next generation SOFC. Electrochim. Acta *193*, 225–230.

Dong, X., Tian, L., Li, J., Zhao, Y., Tian, Y., and Li, Y. (2014). Single layer fuel cell based on a composite of Ce0.8Sm0.2O2-δ–Na2CO3 and a mixed ionic and electronic conductor Sr2Fe1.5Mo0.5O6−δ. J. Power Sources *249*, 270–276.

Duan, C., Huang, J., Sullivan, N., and O'Hayre, R. (2020). Proton-conducting oxides for energy conversion and storage. Appl. Phys. Rev. *7*, 011314.

Duan, C., Kee, R., Zhu, H., Sullivan, N., Zhu, L., Bian, L., Jennings, D., and O'Hayre, R. (2019). Highly efficient reversible protonic ceramic electrochemical cells for power generation and fuel production. Nat. Energy *4*, 230–240.

Duan, C., Tong, J., Shang, M., Nikodemski, S., Sanders, M., Ricote, S., Almansoori, A., and O'Hayre, R. (2015). Readily processed protonic ceramic fuel cells with high performance at low temperatures. Science *349*, 1321–1326.

Dubois, A., Ricote, S., and Braun, R.J. (2017). Benchmarking the expected stack manufacturing cost of next generation, intermediate-temperature protonic ceramic fuel cells with solid oxide fuel cell technology. J. Power Sources *369*, 65–77.

Fabbri, E., Pergolesi, D., and Traversa, E. (2010a). Ionic conductivity in oxide heterostructures: the role of interfaces. Sci. Technol. Adv. Mater. *11*, 054503.

Fabbri, E., Pergolesi, D., and Traversa, E. (2010b). Materials challenges toward proton-conducting oxide fuel cells: a critical review. Chem. Soc. Rev. *39*, 4355–4369.

Fan, L., Ma, Y., Wang, X., Singh, M., and Zhu, B. (2014). Understanding the electrochemical mechanism of the core-shell ceria-LiZnO nanocomposite in a low temperature solid oxide fuel cell. J. Mater. Chem. A *2*, 5399–5407.

Fan, L., Wang, C., Chen, M., and Zhu, B. (2013). Recent development of ceria-based (nano) composite materials for low temperature ceramic fuel cells and electrolyte-free fuel cells. J. Power Sources *234*, 154–174.

Fan, L., Wang, C., Osamudiamen, O., Raza, R., Singh, M., and Zhu, B. (2012). Mixed ion and electron conductive composites for single component fuel cells: I. Effects of composition and pellet thickness. J. Power Sources *217*, 164–169.

Fan, L., Zhu, B., Su, P.-C., and He, C. (2018). Nanomaterials and technologies for low temperature solid oxide fuel cells: recent advances, challenges and opportunities. Nano Energy *45*, 148–176.

Fop, S., McCombie, K.S., Wildman, E.J., Skakle, J.M.S., Irvine, J.T.S., Connor, P.A., Savaniu, C., Ritter, C., and McLaughlin, A.C. (2020). High oxide ion and proton conductivity in a disordered hexagonal perovskite. Nat. Mater. *19*, 752–757.

Götsch, T., Bertel, E., Menzel, A., Stöger-Pollach, M., and Penner, S. (2018). Spectroscopic investigation of the electronic structure of yttria-stabilized zirconia. Phys. Rev. Mater. *2*, 035801.

Ganesh, K.S., Wang, B., Kim, J.-S., and Zhu, B. (2019). Ionic conducting properties and fuel cell performance developed by band structures. J. Phys. Chem. C *123*, 8569–8577.

Gao, Z., Mogni, L., Miller, E., Railsback, J., and Barnett, S. (2016). A perspective on low-temperature solid oxide fuel cells. Energy Environ. Sci. *9*, 1602–1644.

Grandjean, N., Damilano, B., Dalmasso, S., Leroux, M., gt, M.L., and Massies, J. (1999). Built-in electric-field effects in wurtzite AlGaN/GaN quantum wells. J. Appl. Phys. *86*, 3714–3720.

Harboe, S., Schreiber, A., Margaritis, N., Blum, L., Guillon, O., and Menzler, N.H. (2020). Manufacturing cost model for planar 5 kWel SOFC stacks at Forschungszentrum Jülich. Int. J. Hydrogen Energy *45*, 8015–8030.

He, H., Huang, X., and Chen, L. (2000a). A practice of single layer solid oxide fuel cell. Ionics *6*, 64–69.

He, H., Huang, X., and Chen, L. (2000b). Sr-doped LaInO3 and its possible application in a single layer SOFC. Solid State Ion *130*, 183–193.

He, H., Yu, X., Wu, Y., Mu, X., Zhu, H., Yuan, S., and Yang, D. (2015). 13.7% Efficiency graphene–gallium arsenide Schottky junction solar cells with a P3HT hole transport layer. Nano Energy *16*, 91–98.

Hu, H., Lin, Q., Muhammad, A., and Zhu, B. (2015a). Electrochemical study of lithiated transition metal oxide composite for single layer fuel cell. J. Power Sources *286*, 388–393.

Hu, H., Lin, Q., Zhu, Z., Liu, X., Afzal, M., He, Y., and Zhu, B. (2015b). Effects of composition on the electrochemical property and cell performance of single layer fuel cell. J. Power Sources *275*, 476–482.

Hu, H., Lin, Q., Zhu, Z., Liu, X., and Zhu, B. (2014a). Time-dependent performance change of single layer fuel cell with Li0.4Mg0.3Zn0.3O/Ce0.8Sm0.2O2−δ composite. Int. J. Hydrogen Energy *39*, 10718–10723.

Hu, H., Lin, Q., Zhu, Z., Zhu, B., and Liu, X. (2014b). Fabrication of electrolyte-free fuel cell with Mg0.4Zn0.6O/Ce0.8Sm0.2O2−δ–Li0.3Ni0.6Cu0.07Sr0.03O2−δ layer. J. Power Sources *248*, 577–581.

Huang, P., Horky, A., and Petric, A. (1999). Interfacial reaction between nickel oxide and Lanthanum Gallate during sintering and its effect on conductivity. J. Am. Ceram. Soc. *82*, 2402–2406.

Huang, W., Shuk, P., and Greenblatt, M. (1998). Hydrothermal synthesis and properties of terbium- or praseodymium-doped Ce1−xSmxO2−x/2 solid solutions. Solid State Ion *113–115*, 305–310.

Huang, X., Liu, B., Guan, J., Miao, G., Lin, Z., An, Q., Zhu, X., Wang, W., and Guo, J. (2018). Realization of in-Plane p-n junctions with continuous lattice of a homogeneous material. Adv. Mater. *30*, 1802065.

Huang, Y.H., Dass, R.I., Xing, Z.L., and Goodenough, J.B. (2006). Double perovskites as anode materials for solid-oxide fuel cells. Science *312*, 254–257.

Hwang, H.Y., Iwasa, Y., Kawasaki, M., Keimer, B., Nagaosa, N., and Tokura, Y. (2012). Emergent phenomena at oxide interfaces. Nat. Mater. *11*, 103–113.

Inaba, H., and Tagawa, H. (1996). Ceria-based solid electrolytes. Solid State Ion. *83*, 1–16.

Iwahara, H., Esaka, T., Uchida, H., and Maeda, N. (1981). Proton conduction in sintered oxides and its application to steam electrolysis for hydrogen production. Solid State Ion. *3-4*, 359–363.

Jaiswal, N., Tanwar, K., Suman, R., Kumar, D., Upadhyay, S., and Parkash, O. (2019). A brief review on ceria based solid electrolytes for solid oxide fuel cells. J. Alloys Compd. *781*, 984–1005.

Joo, S., Kwon, O., Kim, K., Kim, S., Kim, H., Shin, J., Jeong, H.Y., Sengodan, S., Han, J.W., and Kim, G. (2019). Cation-swapped homogeneous nanoparticles in perovskite oxides for high power density. Nat. Commun. *10*, 697.

Kamran, Y.-S., MuhammadAli, Mushtaq, N., Rauf, S., Xia, C., and Zhu, B. (2019). The semiconductor SrFe0.2Ti0.8O3-δ-ZnO heterostructure electrolyte fuel cells. Int. J. Hydrogen Energy *44*, 30319–30327.

Kreuer, K.D. (2003). Proton-conducting oxides. Annu. Rev. Mater. Res. *33*, 333–359.

Lan, R., and Tao, S. (2014a). New layered proton-conducting oxides LixAl0.6Co0.4O2 and LixAl0.7Co0.3O2. ChemElectroChem *1*, 2098–2103.

Lan, R., and Tao, S. (2014b). Novel proton conductors in the layered oxide material LixAl0.5Co0.5O2. Adv. Energy Mater. *4*, 1301683.

Li, C., Dong, S., Tang, R., Ge, X., Zhang, Z., Wang, C., Lu, Y., and Yin, L. (2018). Heteroatomic interface engineering in MOF-derived carbon heterostructures with built-in electric-field effects for high performance Al-ion batteries. Energy Environ. Sci. *11*, 3201–3211.

Li, J., Lu, Y., Li, D., Qi, F., Yu, L., and Xia, C. (2020). Effects of P-N and N-N heterostructures and band alignment on the performance of low-temperature solid oxide fuel cells. Int. J. Hydrogen Energy *46*, 9790–9798, https://doi.org/10.1016/j.ijhydene.2020.06.103.

Li, P., Yu, B., Li, J., Yao, X., Zhao, Y., and Li, Y. (2016). A single layer solid oxide fuel cell composed of La2NiO4 and doped ceria-carbonate with H2 and methanol as fuels. Int. J. Hydrogen Energy *41*, 9059–9065.

Li, Y., Zheng, N., Yu, L., Wen, S., Gao, C., Sun, M., and Yang, R. (2019). A simple phenyl group introduced at the tail of alkyl side chains of small molecular acceptors: new strategy to balance the crystallinity of acceptors and miscibility of bulk heterojunction enabling highly efficient organic solar cells. Adv. Mater. *31*, 1807832.

Liu, D., and Kelly, T.L. (2014). Perovskite solar cells with a planar heterojunction structure prepared using room-temperature solution processing techniques. Nat. Photon. *8*, 133–138.

Liu, Q., Qin, H., Raza, R., Fan, L., Li, Y., and Zhu, B. (2012). Advanced electrolyte-free fuel cells based on functional nanocomposites of a single porous component: analysis, modeling and validation. RSC Adv. *2*, 8036–8040.

Liu, W., Pan, W., Luo, J., Godfrey, A., Ou, G., Wu, H., and Zhang, W. (2015a). Suppressed phase transition and giant ionic conductivity in La2Mo2O9 nanowires. Nat. Commun. *6*, 8354.

Liu, Y., Tang, Y., Ma, Z., Singh, M., He, Y., Dong, W., Sun, C., and Zhu, B. (2015b). Flowerlike CeO2 microspheres coated with Sr2Fe1.5Mo0.5Ox nanoparticles for an advanced fuel cell. Sci. Rep. *5*, 11946.

Long, R., Mao, K., Gong, M., Zhou, S., Hu, J., Zhi, M., You, Y., Bai, S., Jiang, J., and Zhang, Q. (2014). Tunable oxygen activation for catalytic organic oxidation: Schottky junction versus plasmonic effects. Angew. Chem. Int. Ed. *126*, 3269–3273.

Lu, Y., Akbar, M., Xia, C., Mi, Y., Ma, L., Wang, B., and Zhu, B. (2020). Catalytic membrane with high ion–electron conduction made of strongly correlated perovskite LaNiO3 and Ce0.8Sm0.2O2-δ for fuel cells. J. Catal. *386*, 117–125.

Lu, Y., Zhu, B., Cai, Y., Kim, J.-S., Wang, B., Wang, J., Zhang, Y., and Li, J. (2016). Progress in electrolyte-free fuel cells. Front. Energy Res. *4*, 17.

Ma, Y., Wang, X., Li, S., Toprak, M.S., Zhu, B., and Muhammed, M. (2010). Samarium-doped ceria nanowires: novel synthesis and application in low-temperature solid oxide fuel cells. Adv. Mater. *22*, 1640–1644.

Mahato, N., Banerjee, A., Gupta, A., Omar, S., and Balani, K. (2015). Progress in material selection for solid oxide fuel cell technology: a review. Prog. Mater. Sci. *72*, 141–337.

Meng, J.-H., Liu, X., Zhang, X.-W., Zhang, Y., Wang, H.-L., Yin, Z.-G., Zhang, Y.-Z., Liu, H., You, J.-B., and Yan, H. (2016). Interface engineering for highly efficient graphene-on-silicon Schottky junction solar cells by introducing a hexagonal boron nitride interlayer. Nano Energy *28*, 44–50.

Meng, Y., Mi, Y., Xu, F., Wang, X., Xia, C., Dong, W., Ji, Y., and Zhu, B. (2017). Low-temperature fuel cells using a composite of redox-stable perovskite oxide La0.7Sr0.3Cr0.5Fe0.5O3-δ and ionic conductor. J. Power Sources *366*, 259–264.

Meng, Y., Wang, X., Xia, C., Wang, B., Dong, W., Ji, Y., and Zhu, B. (2018). High-performance SOFC based on a novel semiconductor-ionic SrFeO3-δ–Ce0.8Sm0.2O2-δ membrane. Int. J. Hydrogen Energy *43*, 12697–12704.

Meng, Y., Wang, X., Zhang, W., Xia, C., Liu, Y.-n., Yuan, M., Zhu, B., and Ji, Y. (2019). Novel high ionic conductivity electrolyte membrane based on semiconductor La0.65Sr0.3Ce0.05Cr0.5Fe0.5O3-δ for low-temperature solid oxide fuel cells. J. Power Sources *421*, 33–40.

Mi, Y.Q., Xia, C., Zhu, B., Raza, R., Afzal, M., and Riess, I. (2018). Experimental and physical approaches on a novel semiconducting-ionic membrane fuel cell. Int. J. Hydrogen Energy *43*, 12756–12764.

Mogensen, M., Sammes, N.M., and Tompsett, G.A. (2000). Physical, chemical and electrochemical properties of pure and doped ceria. Solid State Ion *129*, 63–94.

Mubeen, S., Lee, J., Singh, N., Kramer, S., Stucky, G.D., and Moskovits, M. (2013). An autonomous photosynthetic device in which all charge carriers derive from surface plasmons. Nat. Nanotechnol. *8*, 247–251.

Mushtaq, N., Xia, C., Dong, W., Wang, B., Raza, R., Ali, A., Afzal, M., and Zhu, B. (2019). Tuning the energy band structure at interfaces of the SrFe0.75Ti0.25O3−δ–Sm0.25Ce0.75O2−δ heterostructure for fast ionic transport. ACS Appl. Mater. Interfaces *11*, 38737–38745.

Navarro, L., Marques, F., and Frade, J. (1997). n-Type conductivity in Gadolinia-doped ceria. J. Electrochem. Soc. *144*, 267–273.

Nie, X., Zheng, D., Chen, Y., Wang, B., Xia, C., Dong, W., Wang, X., Wang, H., and Zhu, B. (2019). Processing SCNT (SrCo0.8Nb0.1Ta0.1O3-δ)-SCDC (Ce0.8Sm0.05Ca0.15O2-δ) composite into semiconductor-ionic membrane fuel cell (SIMFC) to operate below 500 °C. Int. J. Hydrogen Energy *44*, 31372–31385.

O'Hayre, R., Cha, S.-W., Colella, W., and Prinz, F.B. (2016). Chapter 4: " cell charge transport. In Fuel Cell Fundamentals (John Wiley & Sons), pp. 117–121.

Oikawa, T., Ohdaira, K., Higashimine, K., and Matsumura, H. (2015). Application of crystalline silicon surface oxidation to silicon heterojunction solar cells. Curr. Appl. Phys. *15*, 1168–1172.

Ormerod, R.M. (2003). Solid oxide fuel cells. Chem. Soc. Rev. *32*, 17–28.

Pan, L., Sun, S., Chen, Y., Wang, P., Wang, J., Zhang, X., Zou, J.J., and Wang, Z.L. (2020). Advances in piezo-Phototronic effect enhanced photocatalysis and Photoelectrocatalysis. Adv. Energy Mater. *10*, 2000214.

Qiao, Z., Xia, C., Cai, Y., Afzal, M., Wang, H., Qiao, J., and Zhu, B. (2018). Electrochemical and electrical properties of doped CeO2-ZnO composite for low-temperature solid oxide fuel cell applications. J. Power Sources *392*, 33–40.

Rauf, S., Zhu, B., Yousaf Shah, M.A.K., Tayyab, Z., Attique, S., Ali, N., Mushtaq, N., Wang, B., Yang, C., and Asghar, M.I. (2020). Application of a triple-conducting heterostructure electrolyte of Ba0.5Sr0.5Co0.1Fe0.7Zr0.1Y0.1O3−δ and Ca0.04Ce0.80Sm0.16O2−δ in a high-performance low-temperature solid oxide fuel cell. ACS Appl. Mater. Interfaces *12*, 35071–35080.

Sata, N., Eberman, K., Eberl, K., and Maier, J. (2000). Mesoscopic fast ion conduction in nanometre-scale planar heterostructures. Nature *408*, 946–949.

Seo, S., Park, I.J., Kim, M., Lee, S., Bae, C., Jung, H.S., Park, N.G., Kim, J.Y., and Shin, H. (2016). An ultra-thin, un-doped NiO hole transporting layer of highly efficient (16.4%) organic-inorganic hybrid perovskite solar cells. Nanoscale *8*, 11403–11412.

Serra, J.M. (2019). Electrifying chemistry with protonic cells. Nat. Energy *4*, 178–179.

Shao, K., Li, F., Zhang, G., Zhang, Q., Maliutina, K., and Fan, L. (2019). Approaching durable single-layer fuel cells: promotion of electroactivity and charge separation via nanoalloy redox exsolution. ACS Appl. Mater. Interfaces *11*, 27924–27933.

Shao, Z.P., and Haile, S.M. (2004). A high-performance cathode for the next generation of solid-oxide fuel cells. Nature *431*, 170–173.

Shen, S., Yang, Y., Guo, L., and Liu, H. (2014). A polarization model for a solid oxide fuel cell with a mixed ionic and electronic conductor as electrolyte. J. Power Sources *256*, 43–51.

Singh, K., Nowotny, J., and Thangadurai, V. (2013). Amphoteric oxide semiconductors for energy conversion devices: a tutorial review. Chem. Soc. Rev. *42*, 1961–1972.

Stambouli, A.B., and Traversa, E. (2002). Solid oxide fuel cells (SOFCs): a review of an environmentally clean and efficient source of energy. Renew. Sustain. Energy Rev. *6*, 433–455.

Steele, B., and Heinzel, A. (2001). Materials for fuel-cell technologies. Nature *414*, 345–352.

Steele, B.C.H. (2000). Appraisal of Ce1-yGdyO2-y/2 electrolytes for IT-SOFC operation at 500°C. Solid State Ion. *129*, 95–110.

Stingaciu, M., Zhu, B., Singh, M., and Johnsson, M. (2012). Single-component fuel cells fabricated by spark plasma sintering. RSC Adv. *2*, 12140–12143.

Su, C., Wang, W., Liu, M.L., Tade, M.O., and Shao, Z.P. (2015). Progress and prospects in symmetrical solid oxide fuel cells with two identical electrodes. Adv. Energy Mater. *5*, 1500188.

Sun, C.W., Alonso, J.A., and Bian, J.J. (2020). Recent advances in perovskite-type oxides for energy conversion and storage applications. Adv. Energy Mater *5*, 1–19, https://doi.org/10.1002/aenm.2020004592000459.

Sunarso, J., Hashim, S.S., Zhu, N., and Zhou, W. (2017). Perovskite oxides applications in high temperature oxygen separation, solid oxide fuel cell and membrane reactor: a review. Prog. Energy Combust. Sci. *61*, 57–77.

Tuller, H.L., and Nowick, A.S. (1977). Small polaron electron transport in reduced CeO2 single crystals. J. Phys. Chem. Sol. *38*, 859–867.

Wachsman, E., and Lee, K. (2011). Lowering the temperature of solid oxide fuel cells. Science *334*, 935–939.

Wang, B., Cai, Y., Xia, C., Kim, J.-S., Liu, Y., Dong, W., Wang, H., Afzal, M., Li, J., and Raza, R. (2017). Semiconductor-ionic membrane of LaSrCoFe-oxide-doped ceria solid oxide fuel cells. Electrochim. Acta *248*, 496–504.

Wang, B., Wang, Y., Fan, L., Cai, Y., Xia, C., Liu, Y., Raza, R., van Aken, P.A., Wang, H., and Zhu, B. (2016a). Preparation and characterization of Sm and Ca co-doped ceria–La0.6Sr0.4Co0.2Fe0.8O3−δ semiconductor–ionic composites for electrolyte-layer-free fuel cells. J. Mater. Chem. A. *4*, 15426–15436.

Wang, G., Wu, X., Cai, Y., Ji, Y., Yaqub, A., and Zhu, B. (2016b). Design, fabrication and characterization of a double layer solid oxide fuel cell (DLFC). J. Power Sources *332*, 8–15.

Wang, B., Zhu, B., Yun, S., Zhang, W., Xia, C., Afzal, M., Cai, Y., Liu, Y., Wang, Y., and Wang, H. (2019). Fast ionic conduction in semiconductor CeO2-δ electrolyte fuel cells. NPG Asia Mater. *11*, 51.

Wang, H., Zhang, L., Chen, Z., Hu, J., Li, S., Wang, Z., Liu, J., and Wang, X. (2014). Semiconductor heterojunction photocatalysts: design, construction, and photocatalytic performances. Chem. Soc. Rev. *43*, 5234–5244.

Wang, M., Duan, J., Yang, X., Wang, Y., Duan, Y., and Tang, Q. (2020). Interfacial electric field enhanced charge density for robust triboelectric nanogenerators by tailoring metal/perovskite Schottky junction. Nano Energy *73*, 104747.

Wang, X., Ma, Y., Raza, R., Muhammed, M., and Zhu, B. (2008). Novel core-shell SDC/amorphous Na2CO3 nanocomposite electrolyte for low-temperature SOFCs. Electrochem. Commun. *10*, 1617–1620.

Wang, Z.L. (2010). Piezopotential gated nanowire devices: Piezotronics and piezo-phototronics. Nano Today *5*, 540–552.

Wilson, J.R., Kobsiriphat, W., Mendoza, R., Chen, H.Y., Hiller, J.M., Miller, D.J., Thornton, K., Voorhees, P.W., Adler, S.B., and Barnett, S.A. (2006). Three-dimensional reconstruction of a solid-oxide fuel-cell anode. Nat. Mater. *5*, 541–544.

Winter, M., and Brodd, R.J. (2004). What are batteries, fuel cells, and supercapacitors? Chem. Rev. *104*, 4245–4270.

Wu, S., Li, L., Wang, W., Yu, D., Liu, W., Wu, X., and Zhang, F. (2015). Study on the front contact mechanism of screen-printed multi-crystalline silicon solar cells. Solar Energy Mater. Solar Cells *141*, 80–86.

Wu, Y., Fan, L., Mushtaq, N., Zhu, B., Afzal, M., Sajid, M., Raza, R., Kim, J.-S., Lin, W.-F., and Lund, P.D. (2020). In Solid Oxide Fuel Cells: From Electrolyte-Based to Electrolyte-free Devices, B. Zhu, R. Raza, L. Fan, and C. Sun, eds. (John Wiley & Sons), pp. 347–378, https://doi.org/10.1002/9783527812790.ch11.

Wu, Y., Liu, L., Yu, X., Zhang, J., Li, L., Yan, C., and Zhu, B. (2018a). Natural hematite ore composited with ZnO nanoneedles for energy applications. Compos. B Eng. *137*, 178–183.

Wu, Y., Zhang, J., Li, L., Wei, J., Li, J., Yang, X., Yan, C., Zhou, C., and Zhu, B. (2018b). Proton conduction and fuel cell using the CuFe-oxide mineral composite based on CuFeO2 structure. ACS Appl. Energy Mater. *1*, 580–588.

Wu, Y., Xia, C., Zhang, W., Yang, X., Bao, Z.Y., Li, J.J., and Zhu, B. (2016). Natural hematite for next-generation solid oxide fuel cells. Adv. Funct. Mater. *26*, 938–942.

Xia, C., Cai, Y., Ma, Y., Wang, B., Zhang, W., Karlsson, M., Wu, Y., and Zhu, B. (2016a). Natural mineral-based solid oxide fuel cell with heterogeneous nanocomposite derived from hematite and rare-earth minerals. ACS Appl. Mater. Interfaces *8*, 20748–20755.

Xia, C., Wang, B., Ma, Y., Cai, Y., Afzal, M., Liu, Y., He, Y., Zhang, W., Dong, W., and Li, J. (2016b). Industrial-grade rare-earth and perovskite oxide for high-performance electrolyte layer-free fuel cell. J. Power Sources *307*, 270–279.

Xia, C., Cai, Y., Wang, B., Afzal, M., Zhang, W., Soltaninazarlou, A., and Zhu, B. (2017a). Strategy towards cost-effective low-temperature solid oxide fuel cells: a mixed-conductive membrane comprised of natural minerals and perovskite oxide. J. Power Sources *342*, 779–786.

Xia, C., Wang, B., Cai, Y., Zhang, W., Afzal, M., and Zhu, B. (2017b). Electrochemical properties of LaCePr-oxide/K2WO4 composite electrolyte for low-temperature SOFCs. Electrochem. Commun. *77*, 44–48.

Xia, C., Mi, Y., Wang, B., Lin, B., Chen, G., and Zhu, B. (2019). Shaping triple-conducting semiconductor BaCo0.4Fe0.4Zr0.1Y0.1O3-δ into an electrolyte for low-temperature solid oxide fuel cells. Nat. Commun. *10*, 1707.

Xia, T., Zhang, W., Murowchick, J., Liu, G., and Chen, X. (2013). Built-in electric field-assisted surface-amorphized Nanocrystals for high-rate lithium-ion Battery. Nano Lett. *13*, 5289–5296.

Xia, Y., Liu, X., Bai, Y., Li, H., Deng, X., Niu, X., Wu, X., Zhou, D., Lv, M., and Wang, Z. (2012). Electrical conductivity optimization in electrolyte-free fuel cells by single-component Ce0.8Sm0.2O2-δ-Li0.15Ni0.45Zn0.4 layer. RSC Adv. *2*, 3828–3834.

Xing, Y., Hu, E., Wang, F., Muhammad, N., Wang, B., Wang, J., Maryam, A., Rasheed, M.N., Asghar, M., and Xia, C. (2020). Cubic silicon carbide/zinc oxide heterostructure fuel cells. Appl. Phys. Lett. *117*, 162105.

Xing, Y., Wu, Y., Li, L., Shi, Q., Shi, J., Yun, S., Akbar, M., Wang, B., Kim, J.-S., and Zhu, B. (2019). Proton shuttles in CeO2/CeO2−δ core–shell structure. ACS Energy Lett *4*, 2601–2607.

Xu, H., Shi, Z.-X., Tong, Y.-X., and Li, G.-R. (2018). Porous microrod arrays constructed by carbon-confined NiCo@NiCoO2 Core@Shell nanoparticles as efficient Electrocatalysts for oxygen evolution. Adv. Mater. *30*, 1705442.

Yang, F., Dong, T., Zhang, X., Liu, J., Tian, W., and Zhang, Y. (2020). Semiconductor ionic Ce0.8Sm0.2O2-δ-Na2CO3 – LiCo0.225Cu0.075Ni0.7O3-δ composite material as electrolyte for low temperature solid oxide fuel cells. Int. J. Hydrogen Energy *45*, 14972–14978.

Yousaf, M., Mushtaq, N., Zhu, B., Wang, B., Akhtar, M.N., Noor, A., and Afzal, M. (2020). Electrochemical properties of Ni0.4Zn0.6Fe2O4 and the heterostructure composites (Ni–Zn ferrite-SDC) for low temperature solid oxide fuel cell (LT-SOFC). Electrochim. Acta *331*, 135349.

Yuan, K., Zhu, Z., Afzal, M., and Zhu, B. (2020a). Electrolyte-Based to Electrolyte-Free Devices. In Solid Oxide Fuel Cells, B. Zhu, R. Raza, L. Fan, and C. Sun, eds., pp. 377–413, https://doi.org/10.1002/9783527812790.ch12.

Yuan, M., Dong, W., Wei, L., Liu, Q., Meng, Y., Wang, X., Wang, B., and Zhu, B. (2020b). Stability study of SOFC using layered perovskite oxide La1.85Sr0.15CuO4 mixed with ionic conductor as membrane. Electrochim. Acta *332*, 135487.

Zhang, G., Zhao, J., Chow, P.C.Y., Jiang, K., Zhang, J., Zhu, Z., Zhang, J., Huang, F., and Yan, H. (2018). Nonfullerene acceptor molecules for bulk heterojunction organic solar cells. Chem. Rev. *118*, 3447–3507.

Zhang, Y., Knibbe, R., Sunarso, J., Zhong, Y., Zhou, W., Shao, Z., and Zhu, Z. (2017). Recent progress on advanced materials for solid-oxide fuel cells operating below 500 degrees C. Adv. Mater. *29*, 1700132.

Zhang, Z., and Yates, J.T., Jr. (2012). Band bending in semiconductors: chemical and physical consequences at surfaces and interfaces. Chem. Rev. *112*, 5520–5551.

Zhao, C., Li, Y., Zhang, W., Zheng, Y., Lou, X., Yu, B., Chen, J., Chen, Y., Liu, M., and Wang, J. (2020). Heterointerface engineering for enhancing the electrochemical performance of solid oxide cells. Energy Environ. Sci. *13*, 53–85.

Zheng, Y.F., Xia, C., Dong, W.J., Li, J.J., and Zhu, B. (2016). Scaling up and characterization of single-layer fuel cells. Energy Technol. *4*, 967–972.

Zhou, Y., Guan, X., Zhou, H., Ramadoss, K., Adam, S., Liu, H., Lee, S., Shi, J., Tsuchiya, M., and Fong, D. (2016). Strongly correlated perovskite fuel cells. Nature *534*, 231–234.

Zhou, Y.S., Wang, K., Han, W., Rai, S.C., Zhang, Y., Ding, Y., Pan, C., Zhang, F., Zhou, W., and Wang, Z.L. (2012). Vertically aligned CdSe nanowire arrays for energy harvesting and piezotronic devices. ACS Nano *6*, 6478–6482.

Zhu, B. (2009). Solid oxide fuel cell (SOFC) technical challenges and solutions from nano-aspects. Int. J. Energy Res. *33*, 1126–1137.

Zhu, B., Fan, L., Zhao, Y., Tan, W., Xiong, D., and Wang, H. (2014). Functional semiconductor-ionic composite GDC-KZnAl/LiNiCuZnOx for single-component fuel cell. RSC Adv. *4*, 9920–9925.

Zhu, B., Fan, L., Deng, H., He, Y., Afzal, M., Dong, W., Yaqub, A., and Janjua, N.K. (2016a). LiNiFe-based layered structure oxide and composite for advanced single layer fuel cells. J. Power Sources *316*, 37–43.

Zhu, B., Huang, Y., Fan, L., Ma, Y., Wang, B., Xia, C., Afzal, M., Zhang, B., Dong, W., and Wang, H. (2016b). Novel fuel cell with nanocomposite functional layer designed by perovskite solar cell principle. Nano Energy *19*, 156–164.

Zhu, B., Lund, P., Raza, R., Ma, Y., Fan, L., Afzal, M., Patakangas, J., He, Y., Zhao, Y., and Tan, W. (2015). Schottky junction effect on high performance fuel cells based on nanocomposite materials. Adv. Energy Mater. *5*, 1401895.

Zhu, B., Lund, P., Raza, R., Patakangas, J., Huang, Q., Fan, L., and Singh, M. (2013). A new energy conversion technology based on nano-redox and nano-device processes. Nano Energy *2*, 1179–1185.

Zhu, B., Raza, R., Abbas, G., and Singh, M. (2011a). An electrolyte-free fuel cell constructed from one homogenous layer with mixed conductivity. Adv. Funct. Mater. *21*, 2465–2469.

Zhu, B., Raza, R., Qin, H., and Fan, L. (2011b). Single-component and three-component fuel cells. J. Power Sources *196*, 6362–6365.

Zhu, B., Raza, R., Qin, H., Liu, Q., and Fan, L. (2011c). Fuel cells based on electrolyte and non-electrolyte separators. Energy Environ. Sci. *4*, 2986–2992.

Zhu, B., Raza, R., Liu, Q., Qin, H., Zhu, Z., Fan, L., Singh, M., and Lund, P. (2012). A new energy conversion technology joining electrochemical and physical principles. RSC Adv. *2*, 5066–5070.

Zhu, B., Wang, B., Wang, Y., Raza, R., Tan, W., Kim, J., van Aken, P., and Lund, P. (2017). Charge separation and transport in La0.6Sr0.4Co0.2Fe0.8O3-δ and ion-doping ceria heterostructure material for new generation fuel cell. Nano Energy *37*, 195–202.